GEORGIA INSTITUTE OF TECHNOLOGY
OFFICE OF CONTRACT ADMINISTRATION
SPONSORED PROJECT INITIATION

Date: 1/31/79

Project Title: The Effect of Microstructure on the Properties of High Strength Aluminum Alloys. Green Card

Project No: E-19-674 (continuation of E-19-659)

Project Director: Dr. E. A. Starke

Sponsor: Air Force Office of Scientific Research

Agreement Period: From 1/1/79 Until 12/31/79 (02 Year)

Type Agreement: Grant No. AFOSR-78-3471A & B

Amount: $127,739 AFOSR
16,889 GIT (E-19-343)
$144,628 TOTAL

Reports Required: Interim Technical Reports; Final Technical Report

Sponsor Contact Person (s):

Technical Matters

Dr. Alan H. Rosenstein
Program Manager
Directorate of Electronic & Solid State Sciences
Building 410
Bolling AFB, D. C. 20332

Contractual Matters
(thru OCA)

Ms. Joan O. Marshall
Contracting Officer
Air Force Office of Scientific Research
Building 410
Bolling AFB, D. C. 20332

Defense Priority Rating: N/A

Assigned to: Chemical Engineering (School/Laboratory)

COPIES TO:

Project Director
Division Chief (EES)
School/Laboratory Director
Dean/Director–EES
Accounting Office
Procurement Office
Security Coordinator (OCA)
Reports Coordinator (OCA)

Library, Technical Reports Section
EES Information Office
EES Reports & Procedures
Project File (OCA)
Project Code (GTRI)
Other

CA–3 (3/76)

GEORGIA INSTITUTE OF TECHNOLOGY
OFFICE OF CONTRACT ADMINISTRATION

SPONSORED PROJECT TERMINATION

Date: June 11, 1980

Project Title: The Effect of Microstructure on the Properties of High Strength Aluminum Alloys.

Project No: E-19-674

Project Director: Dr. E. A. Starke

Sponsor: Air Force Office of Scientific Research

Effective Termination Date: 12/31/79 (continued under E-19-603)

Clearance of Accounting Charges: 12/31/79

Grant/Contract Closeout Actions Remaining:

_ Final Invoice and Closing Documents
x ~~Final~~ Fiscal Report (Interim)
_ Final Report of Inventions
x Govt. Property Inventory & Related Certificate
_ Classified Material Certificate
_ Other _____

Assigned to: Chemical Engineering (School/~~Laboratory~~)

COPIES TO:

Project Director
Division Chief (EES)
School/Laboratory Director
Dean/Director–EES
Accounting Office
Procurement Office
Security Coordinator (OCA)
Reports Coordinator (OCA)

Library, Technical Reports Section
EES Information Office
Project File (OCA)
Project Code (GTRI)
Other C. E. Smith

CA–4 (1/79)

FINANCIAL STATUS REPORT

(Follow instructions on the back)

1. FEDERAL AGENCY AND ORGANIZATIONAL ELEMENT TO WHICH REPORT IS SUBMITTED	2. FEDERAL GRANT OR OTHER IDENTIFYING NUMBER	OMB Approved No. 80-R0180	PAGE	OF
Air Force Office of Scientific Research	AFOSR-78-3471		1	1 PAGES

3. RECIPIENT ORGANIZATION (Name and complete address, including ZIP code)	4. EMPLOYER IDENTIFICATION NUMBER	5. RECIPIENT ACCOUNT NUMBER OR IDENTIFYING NUMBER	6. FINAL REPORT	7. BASIS
Georgia Institute of Technology Atlanta, Georgia 30332	58-6002023	E-19-674	☐ YES ☒ NO	☒ CASH ☐ ACCRUAL

8. PROJECT/GRANT PERIOD (See instructions)		9. PERIOD COVERED BY THIS REPORT	
FROM (Month, day, year)	TO (Month, day, year)	FROM (Month, day, year)	TO (Month, day, year)
1/1/79	12/31/79	1/1/79	12/31/79

10. STATUS OF FUNDS

PROGRAMS/FUNCTIONS/ACTIVITIES ▶	(a) Personal Services	(b) Retirement Benefits	(c) Materials & Supplies	(d) Travel	(e) Capital Outlay	(f) Overhead	TOTAL (g)
a. Net outlays previously reported	$ 45,413.77	$ 3,247.27	$ 2,099.50	$ 507.15	$	$ 30,881.36	$ 82,149.05
b. Total outlays this report period	75,295.00	5,095.52	3,930.94	1,631.76	1,500.00	57,224.20	144,677.42
c. *Less:* Program income credits							
d. Net outlays this report period *(Line b minus line c)*	75,295.00	5,095.52	3,930.94	1,631.76	1,500.00	57,224.20	144,677.42
e. Net outlays to date *(Line a plus line d)*	120,708.77	8,342.79	6,030.44	2,138.91	1,500.00	88,105.56	226,826.47
f. *Less:* Non-Federal share of outlays	18,880.00	1,673.40				13,574.80	34,128.20
g. Total Federal share of outlays *(Line e minus line f)*	101,828.77	6,669.39	6,030.44	2,138.91	1,500.00	74,530.76	192,698.27
h. Total unliquidated obligations							
i. *Less:* Non-Federal share of unliquidated obligations shown on line h							
j. Federal share of unliquidated obligations							
k. Total Federal share of outlays and unliquidated obligations	101,828.77	6,669.39	6,030.44	2,138.91	1,500.00	74,530.76	192,698.27
l. Total cumulative amount of Federal funds authorized	101,911.00	6,480.00	6,078.00	2,200.00	1,500.00	74,570.00	192,739.00
m. Unobligated balance of Federal funds	82.23	(189.39)	47.56	61.09		39.24	40.73

11. INDIRECT EXPENSE

a. TYPE OF RATE *(Place "X" in appropriate box)* ☐ PROVISIONAL ☒ PREDETERMINED ☐ FINAL ☐ FIXED

b. RATE	c. BASE	d. TOTAL AMOUNT	e. FEDERAL SHARE
To 6/30/78 68% As of 7/1/78 76%	Salaries & Wages	$88,105.56	$74,530.76

12. REMARKS: *Attach any explanations deemed necessary or information required by Federal sponsoring agency in compliance with governing legislation.*

13. CERTIFICATION

I certify to the best of my knowledge and belief that this report is correct and complete and that all outlays and unliquidated obligations are for the purposes set forth in the award documents.

SIGNATURE OF AUTHORIZED CERTIFYING OFFICIAL

DATE REPORT SUBMITTED

TYPED OR PRINTED NAME AND TITLE
David V. Welch, Manager, Grants & Contracts Accounts

TELEPHONE *(Area code, number and extension)*
404/894-4624

269-102

STANDARD FORM 269 (7-76)
Prescribed by Office of Management and Budget
Cir. No. A-110

E-19-674

SECURITY CLASSIFICATION OF THIS PAGE *(When Data Entered)*

REPORT DOCUMENTATION PAGE		READ INSTRUCTIONS BEFORE COMPLETING FORM
1. REPORT NUMBER	2. GOVT ACCESSION NO.	3. RECIPIENT'S CATALOG NUMBER
4. TITLE *(and Subtitle)* The Effect of Microstructure on The Properties of High Strength Aluminum Alloys		5. TYPE OF REPORT & PERIOD COVERED Annual Report, 1/1/79-12/31/79 6. PERFORMING ORG. REPORT NUMBER
7. AUTHOR(s) Edgar A. Starke, Jr. and T. H. Sanders, Jr.		8. CONTRACT OR GRANT NUMBER(s) AFOSR-78-3471
9. PERFORMING ORGANIZATION NAME AND ADDRESS Fracture and Fatigue Research Laboratory Georgia Institute of Technology Atlanta, GA 30332		10. PROGRAM ELEMENT, PROJECT, TASK AREA & WORK UNIT NUMBERS
11. CONTROLLING OFFICE NAME AND ADDRESS Electronic & Solid State Sciences Air Force Office of Scientific Research Bolling AFB, Building 410 Washington, DC. 20332		12. REPORT DATE March 13, 1980 13. NUMBER OF PAGES 60
14. MONITORING AGENCY NAME & ADDRESS *(if different from Controlling Office)*		15. SECURITY CLASS. *(of this report)* Unclassified 15a. DECLASSIFICATION/DOWNGRADING SCHEDULE

16. DISTRIBUTION STATEMENT *(of this Report)*

Unlimited

17. DISTRIBUTION STATEMENT *(of the abstract entered in Block 20, if different from Report)*

18. SUPPLEMENTARY NOTES

19. KEY WORDS *(Continue on reverse side if necessary and identify by block number)*

20. ABSTRACT *(Continue on reverse side if necessary and identify by block number)*

This program was initiated on 1 January 1979, the effect of copper content on the FCP behavior of four Al-6Zn-2Mg-XCu-T7351 alloys was investigated in dry air and distilled water and compared with last year's study of the T651 condition. The peak-aged-treatment exhibited a lower growth rate in dry air over the range of ΔK studied, and also displayed a higher threshold and resistance to fatigue cracking near the threshold in the distilled water environment. This suggests that age hardened alloys with planar slip (dislocation

DD FORM 1 JAN 73 1473

SECURITY CLASSIFICATION OF THIS PAGE *(When Data Entered)*

shearing mechanism) will have a higher threshold than those having wavy and/or homogeneous slip. The shape of the growth rate curves can be correlated best with a transition in the fracture surface appearance which is controlled by the deformation behavior. The copper content of the four alloys in the over-aged condition did not significantly affect the growth rate in either dry air or distilled water. However, in distilled water there were minor differences in the form of the growth rate curves with copper content. This is associated with electrochemical potential differences at the crack tip among the four alloys. The environmental sensitivity of the peak-aged condition was several times higher than the over-aged treatment at the higher ΔK's and the sensitivity of the former condition was much more dependent upon the copper content. This behavior is considered to be due to strain localization which occurs in the peak-aged condition and which enhances the metal-environment interactions.

Increasing the copper content to the Al-Zn-Mg alloys in the T651 condition was found to improve the SCC resistance. The improvement in region I of the $v\text{-}K_1$ curve is associated with the change in the deformation mode of the alloy. The effect of copper in strongly improving the region II kinetics is attributed to the electrochemical factors. The copper addition may also affect the region II cracking by reducing the rate of transport of hydrogen as the homogeneity of deformation improves.

To test the hypothesis that elements such as sodium are deleterious to the fracture behavior of precipitation hardening Al-Li alloys, five Al-3 weight per cent lithium alloys were cast. The sodium levels varied from 10 to 800 ppm. The time dependent growth of precipitate free zones (PFZ's) during the isothermal aging of Al-Li and Al-Li-Mg is being studied and will be related to the fracture behavior. A TEM investigation on the deformation structure of fractured tensile specimens of 2020 showed that when the failure process was predominately transgranular the slip band length was modified by the presence of manganese dispersoids ($Al_{20}Mn_3Cu_2$). However, when the slip band transveresed the grain, the fracture was predominately intergranular. The corrosion behavior of Al-3% Li alloy sheet is being investigated. The corrosion potential and the anodic and cathodic polarization curves have been obtained. The results indicate that there is an increase in the corrosion rate corresponding with increasing isothermal aging time. This phase of the program is in its initial stages.

THE EFFECT OF MICROSTRUCTURE ON THE PROPERTIES OF HIGH STRENGTH ALUMINUM ALLOYS

AFOSR Annual Scientific Report
February 1980

by

Edgar A. Starke, Jr. and T. H. Sanders, Jr.
Fracture and Fatigue Research Laboratory
Georgia Institute of Technology
Atlanta, Georgia 30332

This Research was sponsored by the Air Force Office of Scientific Research Directorate of Electronics and Solid State Sciences under Research Grant Number AFOSR-78-3471

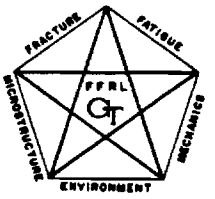

TABLE OF CONTENTS

ABSTRACT

This program was initiated on 1 January 1978. During 1979, the effect of copper content on the FCP behavior of four Al-6Zn-2Mg-XCu-T7351 alloys was investigated in dry air and distilled water and compared with last year's study of the T651 condition. The peak-aged-treatment exhibited a lower growth rate in dry air over the range of ΔK studied, and also displayed a higher threshold and resistance to fatigue cracking near the threshold in the distilled water environment. This suggests that age hardened alloys with planar slip (dislocation shearing mechanism) will have a higher threshold than those having wavy and/or homogeneous slip. The shape of the growth rate curves can be correlated best with a transition in the fracture surface appearance which is controlled by the deformation behavior. The copper content of the four alloys in the over-aged condition did not significantly affect the growth rate in either dry air or distilled water. However, in distilled water there were minor differences in the form of the growth rate curves with copper content. This is associated with electrochemical potential differences at the crack tip among the four alloys. The environmental sensitivity of the peak-aged condition was several times higher than the over-aged treatment at the higher ΔK's and the sensitivity of the former condition was much more dependent upon the copper content. This behavior is considered to be due to strain localization which occurs in the peak-aged condition and which enhances the metal-environment interactions.

Increasing the copper content to the Al-Zn-Mg alloys in the -T651 condition was found to improve the SCC resistance. The improvement in region I of the v-K_1 curve is associated with the change in the deformation mode of the alloy. The effect of copper in strongly improving the region II kinetics is attributed

to the electrochemical factors. The copper addition may also affect the region II cracking by reducing the rate of transport of hydrogen as the homogeneity of deformation improves.

To test the hypothesis that elements such as sodium are deleterious to the fracture behavior of precipitation hardening Al-Li alloys, five Al-3 weight per cent lithium alloys were cast. The sodium levels varied from 10 to 800 ppm. The time dependent growth of precipitate free zones (PFZ's) during the isothermal aging of Al-Li and Al-Li-Mg is being studied and will be related to the fracture behavior. A TEM investigation on the deformation structure of fractured tensile specimens of 2020 showed that when the failure process was predominately transgranular the slip band length was modified by the presence of manganese dispersoids ($Al_{20}Mn_3Cu_2$). However, when the slip band transversed the grain, the fracture was predominately intergranular. The corrosion behavior of Al-3% Li alloy sheet is being investigated. The corrosion potential and the anodic and cathodic polarization curves have been obtained. The results indicate that there is an increase in the corrosion rate corresponding with increasing isothermal aging time. This phase of the program is in its initial stages.

I. FATIGUE CRACK GROWTH BEHAVIOR OF Al-6Zn-2Mg-XCu ALLOYS:

Many structural materials fail by corrosion fatigue if they are exposed to an aggressive environment while undergoing cyclic loading. It is apparent that the consideration of corrosion fatigue characteristics associated with the intended service environment is a primary factor in evaluating and selecting materials to resist fatigue cracking. The corrosion fatigue behavior is controlled by microstructural features which control deformation processes. In order to improve the resistance to corrosion fatigue cracking, one must determine which parameters control the process and whether or not they can be modified by metallurgical manipulations.

Many early fatigue studies relied on S/N curves which show the relationship between the number of cycles to failure and the applied stress. This testing procedure combines fatigue crack initiation and propagation. Since materials may contain inherent flaws associated with processing and/or manufacturing procedures, the useful life of many structures may be dominated by fatigue crack propagation (FCP); especially in the range close to the threshold, ΔK_{th}. FCP has been described by continuum fracture mechanics, and the empirical Paris power law[1] relates the growth rate da/dN, to the stress intensity range, ΔK. Normally the da/dN-ΔK curve can be divided into three regimes[2-4]: Regime I, which is considered microstructurally sensitive; Regime II, which is considered microstructurally insensitive; and, Regime III, which is again microstructurally sensitive.

Data published in the past decade has related the fatigue crack growth rate (FCGR) of aluminum alloys to such variables as mean stress, microstructure, frequency of testing, and environment, etc.[5-10] However, most results were obtained in Regime II. Only a few publications have been concerned with FCGR at low ΔK's[6,10,11]. The FCP behavior near the ΔK_{th} range has been paid

comparatively little attention since the time necessary for obtaining accurate data is large. However, the FCGR in this region is important to engineering design and life predictions of airframe structures. Studies in this region are also essential in order to understand the growth mechanism at low ΔK's and the microstructural-load-environment influence on ΔK_{th}.

The aim of this phase of our program is to characterize the effect of copper content and precipitate structure of Al-6Zn-2Mg-XCu aluminum alloys on the FCGR for the low ΔK range in dry air and distilled water. The test specimens were processed to obtain similar sizes of unrecrystallized grains and subgrains; similar degree of recrystallization (DR), and the same inclusion content. The copper content and precipitate structure are thus isolated and are the major variables evaluated.

EXPERIMENTAL PROCEDURES

Four Al-6Zn-2Mg-XCu alloys with 0, 1.0, 1.6 and 2.1% Cu and having almost identical grain structures were chosen to study the effect of copper content on the FCGR in dry air and distilled water. The chemical composition of the alloys are given in Table 1. The manufacturing processes, the methods for determining the volume percent recrystallized, and the grain and subgrain size have been described previously.[12] All specimens were solutionized at 480°C, stretched 1.5% and aged 24 hours at 120°C to produce the T651 condition. Some specimens were overaged 32, 30, 27 and 12 hours at 150°C for the 2, 1.6, 1, and 0% Cu alloys respectively. This resulted in a hardness equivalent to 85% of the T651 condition, and may be designated T7351.

Compact-tension-type FCP samples were cut from the aged plates with the starter notches parallel to the rolling direction and a T-L crack plane orientation. The samples were 7.4 mm thick and had a H/W of 0.6. FCP tests were performed on a closed-loop servohydraulic machine using tension-tension

loading, a minimum-maximum load ratio of 0.1 and a frequency of 10 Hz. Thresholds, ΔK_{th}, were approached using a successive load reduction with about 10% reduction in K_{max} at each step. Measurements were taken for each load level. The incremental crack length was 50-100 times larger than the maximum plastic zone size of the previous loading. The ΔK_{th} values were obtained in terms of the stress intensity at which only about 0.1 mm growth occurred for $7X10^5$ cycles ($\simeq 1X10^{-10}$ m/cycle). After completion of the threshold measurements, the load was increased in steps and the same procedure followed. When the ΔK reached about 7 $MPam^{\frac{1}{2}}$, the load was kept constant and the ΔK increased with increasing length. The crack length was measured with a travelling microscope to an accuracy of $\pm$ 0.01 mm. The secant method[13] was used to calculate the growth rate. The fracture surfaces of selected FCP specimens were examined by SEM.

Electrochemical potential measurements were made in the vicinity of the crack tip. A hole with diameter and depth of 3 mm was drilled just behind the crack tip and a salt bridge was connected directly to this hole. The other area of specimen was coated with Silicone Rubber RTV 102. Distilled water, acidified to a pH of 3.5 with H_2SO_4, was used for the bulk solution. The solution was acidified to increase its conductivity, and the value of 3.5 was selected to correspond to the value found at the crack tip in SCC experiments.[14] A neutral 3.5% NaCl solution was also used for a series of measurements. The effect of test frequency (between 0.01 and 10 Hz) and the stress intensity range (between 5.0 and 15.0 $MPam^{\frac{1}{2}}$) on the electrode potential at the crack tip was determined. The change in distance between the measuring point and the crack tip during the various tests was insignificant compared to the magnitude of the difference in ΔK investigated.

EXPERIMENTAL RESULTS AND DISCUSSION

Monotonic Mechanical Properties

The mechanical properties of the four alloys are presented in Table 2, along with their degree of recrystallization (volume percent recrystallized), subgrain size and unrecrystallized grain size. Since the microstructural parameters and inclusion content (derived from the table of alloy composition) were similar, the copper content was the major variable. The monotonic properties of the alloys were also similar; with approximately ten percent variation from the minimum to the maximum. The variation in properties can be accounted for by an increase in the volume percent of precipitates present as the copper content is increased.

The deformation behavior of the T651 condition has been described previously[12], and depends on the copper content. The addition of copper not only increases the volume fraction of strengthening precipitates, but also increases the number of partially coherent and incoherent precipitates and thus the homogeneity of deformation. Consequently, in the T651 condition, the strengthening precipitates are sheared in the copper-lean alloys and looped in the copper-rich alloys. This results in inhomogeneous deformation and strain localization for the former, and homogeneous deformation of the latter. On the other hand, when the alloys are aged to the T7351 condition, the strengthening precipitates are partially-coherent and/or incoherent for all alloys and deformation occurs by a looping mechanism regardless of the copper content.[15,16].

Effect of Copper Content, Microstructure, and Environment on ΔK_{th}

The ΔK_{th} was taken as the ΔK corresponding to a growth rate of $1X10^{-10}$ m/cycle since the da/dN vs. ΔK curve for this growth rate was essentially

parallel to the ordinate. The values are presented in Table 3 for both the dry air and H_2O tests. The values obtained for the four alloys in the T7351 condition tested in dry air were the same $\sim$ 2.6 $MPam^{\frac{1}{2}}$. This is due to the similarities in microstructure and deformation modes. The values are lower for the distilled water test, and there is a slight variation with copper content. However, this variation is probably insignificant, and may be due to local environmental effects. The ΔK_{th} for the 1% Cu alloy in the T651 condition is slightly higher than the T7351 value in both dry air and distilled water. We believe this is due to a higher degree of reversibility of slip, since the deformation mode is planar for the T651 treatment. It may also be associated with the extensive crack branching observed at low ΔK's for this alloy and aging treatment.[17]

Fatigue Crack Growth Behavior in Dry Air

The Effect of Aging Treatment and Copper Content: The crack growth rate data for the four alloys in the T7351 condition are presented in Figure 1. The curves for the T651 treatment, obtained from a previous study,[17] are also included in order to compare the effect of aging condition, and deformation behavior, on the FCGR. The crack growth measurements were repeated for the 1.0% Cu alloy in the T651 condition since our previous study did not cover the ΔK range of this investigation. Figure 1 shows that for the T651 condition the crack growth rates increase with increasing copper content regardless of the stress intensity factor. However, for the T7351 condition the crack growth rates are independent of copper content--at least in the dry air environment.

In the T651 condition, the coherency of the strengthening precipitates decreases with increasing copper content and this alters the deformation mode

and subsequent fracture path with respect to the "copper-lean" alloys.[17] Our earlier study showed that zig-zag crack growth and crack branching increased with decreasing copper content, and we attributed this phenomenon to the higher probability of precipitate shearing for the lower copper content alloys. Dislocation shearing of precipitates promotes coarse planar slip and inhomogeneous deformation (strain localization[15]) which favors slip plane decohesion and the occurrance of zig-zag growth and crack branching. The incoherent precipitates of the higher copper content alloys are looped by dislocations promoting more homogeneous slip, noncrystallographic fracture and a single, straight running crack lying in a plane normal to the stress axis. The da/dN was found to decrease (for any chosen calculated ΔK) as the fracture path changed from a single straight crack to a zig-zag crack, to a crack with numerous branches.

The above explanation explains the relative position, with respect to Cu content, of the da/dN-ΔK curves for the T651 condition. It also suggests that the crack growth rate would increase with overaging--i.e., for the T7351 treatment--since for this aging condition the strengthening precipitates are looped by the dislocations and deformation is relatively homogeneous. In addition, the fatigue crack growth rates should be insensitive to copper content since no difference in deformation behavior occurs, with respect to copper content, for the T7351 condition. The results shown in Figure 1 support this interpretation.

The Shape of the da/dN-ΔK Curve and the Related Fracture Mode: At first observation, the da/dN-ΔK curves of Figure 1 appear to follow the normal three-regime crack growth behavior described in the Introduction. However, no data was collected close to the fracture toughness or under plane stress--i.e., in

Regime III--for these alloys. The K_Q values for the 7.4 mm thick plate used in this study are about twice the K_{IC} values shown in Table 2. For the T7351 condition, Regime II can be considered to occur for ΔK's above 5 $MPam^{\frac{1}{2}}$ ($da/dN \simeq$ 0.004 μm/cycle). However, for ΔK's below this value the crack growth rates did not make a smooth transition to a ΔK_{th} (normally considered Regime I), as anticipated. Below 5 $MPam^{\frac{1}{2}}$ the slope of the da/dN-ΔK curve decreased, i.e., an incremental decrease in ΔK did not result in as large of a decrease in da/dN as predicted by either extending the Paris region (Regime II) or approaching a threshold ΔK. Below a ΔK of 3 $MPam^{\frac{1}{2}}$ the FCGR dropped sharply and a ΔK_{th} was obtained. Makay[18] has recently observed similar anomolous behavior for 2024-T3 and 7075-T6.

An analogous slope change is observed in the da/dN-ΔK curves from our previous study of the T651 condition, Figure 1. For this aging treatment the slope change occurred at different ΔK values for the different copper-content alloys--with ΔK decreasing with increasing copper content. The slope change was associated with a transition from homogeneous to inhomogeneous deformation as the ΔK decreased. Therefore, this transition occurs at higher ΔK's for alloys having shearable precipitates, than for alloys having nonshearable (i.e., incoherent) precipitates. Likewise, the transition should occur at lower ΔK's for alloys in the T7351 condition and should be independent of copper content, as observed in Figure 1.

SEM observations of the fracture surface of the alloys in the T7351 condition indicate that transitions in the slope of the FCGR curves could also be correlated with transitions in fracture mode. Features corresponding to different regions of the da/dN-ΔK curves are shown in Figure 2. At low ΔK's near the threshold region and up to 3 $MPam^{\frac{1}{2}}$, the fracture surfaces

were crystallographic in nature and exhibited large facets which covered the unrecrystallized grains, Figure 2a. The facets were either featureless or had parallel markings running normal to the crack propagation direction and terminating at unrecrystallized grain boundaries. The spacing of these markings was much too large to correspond to the advance of the crack during each cycle. Similar features have been observed by Feeney et al.[10] and Hertzberg and Mills[19] who suggested that they may represent different levels along which the crack has propagated, or slip offsets produced in the wake of the crack front. We believe they are due to coarse slip-band offsets. Visual observation revealed a shiny shear lip in this region which made an angle of 30°-50° with respect to the stress axis. This suggests that crack propagation close to ΔK_{th} is similar to Stage I crack propagation, i.e., slip plane decohesion and involves only a few slip systems. The result of the formation of a Stage I type crack decreases both the effective stress intensity and the crack tip opening displacement since the crack tip geometry is not symmetrical.

Between ΔK's of 3 and 5 $MPam^{\frac{1}{2}}$ (the "bump" region of the FCGR curve) the fracture surface was composed of multiple facets, smaller than the unrecrystallized grains, but larger than the subgrains, Figure 2b. Most facets contained coarse slip markings. In this region slip is less restricted than that below a ΔK of 3 $MPam^{\frac{1}{2}}$ but more restricted than for ΔK's > 5 $MPam^{\frac{1}{2}}$. At low ΔK's slip may be restricted either because the critical resolved shear stress is not exceeded on conjugate or cross slip systems or by the constraints of the small ($\sim$ 1-2 μm) plastic zone. We believe that multifaced crack growth is due to restricted slip and is not a result of cleavage. Cracking may occur simultaneously in numerous areas of the same grain of the plastic zone and all cracks may not be on parallel crystallographic planes. The observed multifaced appearance

results from link up of numerous cracks. Chakrabortty and Starke[20] have used a similar explanation for the multifaceted crack growth observed in Ti-V alloys.

At ΔK's > 5 $MPam^{\frac{1}{2}}$ the fracture surface is noncrystallographic. Figure 2c and 2d. Here multiple slip occurs and the crack growth is due to a "plastic blunting" mechanism similar to the one proposed by Laird and co-workers[21,22]. The geometry of the "plastic blunting" process dictates that the fracture plane be perpendicular to the loading direction, as observed for this region of the da/dN-ΔK curve.

Similar fracture features were observed for alloys aged to the T651 condition. Figure 3 (a-d) are scanning electron micrographs of the fracture surface of the alloy represented in Figure 2, but aged to the T651 condition. The fracture features show the same trends with respect to the different sections of the da/dN-ΔK curve. The similarity in fracture appearance suggests that planar slip is prevalent at low ΔK regardless of the aging condition. The slower crack growth rate of the T651 condition at low ΔK may be associated with a higher degree of slip reversibility.[23-24] Slip is probably more reversible for the T651 condition which has shearable precipitates, than for the T7351 condition which has non-shearable precipitates. In order to study the deformation behavior of the FCP samples at low ΔK's, thin foils for TEM were prepared from close to the fracture surface. However, no deformation structure was observed; possibly due to the experimental difficulty of obtaining part of the small ($\sim$ 1 μm) plastic zone in the thinned region of the foil.

Fatigue Crack Growth Behavior in Distilled H_2O

The Effect of Aging Treatment and Copper Content: The distilled water crack growth rate data for the four alloys in the T7351 condition are presented

in Figure 4. The curves for the T651 treatment, obtained from a previous study are shown for comparison. As mentioned before, the crack growth measurements were repeated for the 1% Cu alloy in the T651 condition since our current study covers a lower ΔK range. The T651 condition contains a large volume fraction of shearable precipitates which enhances coarse planar slip and leads to strain localization.[12] The strain localization affects the crack propagation in two ways; it intensifies metal-environment interactions and thus accelerates crack propagation in aggressive environments, but it also favors slip plane decohesion, which leads to zig-zag crack growth, and crack branching, both of which slow down crack propagation.[17] It appears that below ΔK's of 7 $MPam^{\frac{1}{2}}$ the effect of crack branching dominates and the FCGR for the T651 condition is slower than that of the T7351 condition, as clearly shown in Figure 4b. However, for ΔK's above this value the crack-growth rates are similar with the T7351 being actually slower for a particular ΔK. This convergence is expected since our previous study showed that the probability of zig-zag crack growth and crack branching decreases with increasing ΔK.

The amount of plasticity necessary for a particular increment of crack propagation is decreased in aggressive environments,[25] and analogous to our previous results for the T651 condition,[17] distilled water accelerates fatigue crack propagation over that of dry air at equivalent ΔK's, Figure 5. However, the effect is much less drastic for T7351 than for T651, as can be seen from the ratio of the FCGR in H_2O to that in dry air, Table 4. Lifta and Sprowls[26] have shown that the electrochemical potential of 7XXX alloys shifts in the anodic direction when going from the T651 to the T7351 condition. This change in the electrochemical properties coupled with the more homogeneous deformation of the overaged alloys probably account for the decrease in environmental sensitivity.

Unlike the dry air curves for the T7351 condition, the distilled water curves do show slight differences with copper content. The slopes of the curves in the region of highest environmental sensitivity--i.e., for ΔK's between $\sim$ 4 and 8 $MPam^{\frac{1}{2}}$--decrease with increasing copper content, Table 5. Eventually, the aggressive environment da/dN-ΔK curves should converge with those of dry air since at large ΔK's plasticity effects dominate and occur too rapidly for chemical effects to be important.[27] When this happens there is a decrease in the slope of the da/dN-ΔK curves. Table 5 shows that the ΔK for this occurrence increases with decreasing copper content.

The electrode potential at the crack tip was more noble as the copper content increased--the measured values being -0.824, -0.804, -0.752, and -0.715 volts for the 0%, 1.0%, 1.6%, and 2.1% Cu alloys when using acidified H_2O. The same trend was observed when using a neutral NaCl solution with the only difference being a more negative value for each alloy (by $\sim$ 0.15 volts). The potential was independent of load direction, stress intensity range, and frequency--at least for frequencies between 0.01 and 10 Hz. This suggests that fresh metal is created in both the tensile and compressives strokes and remains active. Consequently, the corrosion FCP behavior of these alloys is probably not related to passivation rates or oxide film rupture, but is more likely controlled by solution transport to the crack tip, the kinetics of the electrochemical reactions at the crack tip, and the diffusion of hydrogen into the plastic zone.[28] The major difference in these parameters with respect to copper content is most likely the kinetics of the electrochemical reactions. More hydrogen/cycle is produced for the less noble alloys. The hydrogen atoms may then diffuse into the plastic zone decreasing the amount of plasticity needed for fracture.[28]

The Shape of These da/dN-ΔK Curves and the Related Fracture Mode: The shape of the FCGR curves for the four alloys in the T7351 condition tested in distilled water are similar to those of the dry air tests for the low ΔK range (compare Figures 1 and 4). There is also a very similar relationship between the fracture surface appearance and the shape of the growth rate curves. Compare, for example, Figures 6 and 7 with Figures 2 and 3. Our previous interpretation of this relationship also applies here. The major difference between the fracture features of dry air and distilled water tests is the larger amount of flat featureless regions with cleavage-like patterns on the fracture surface of the distilled water samples. As mentioned before, we believe this is a result of the environment reducing the amount plasticity required for fracture.

The shape of the growth rate curves has been shown to be dependent upon R ratio, microstructure, environment, load history, and their interaction.[29] For ΔK's below $\sim$ 7 MPam$^{\frac{1}{2}}$, we have shown that the growth rate curves are very similar for different microstructures (i.e., for the T651 and T7351) and different environments, (i.e., H_2O and dry air). Figure 8 shows that the shape of the curves is independent of R ratio; at least for R's of 0.5 to 0.1. The slope change which we associate with a transition from environmentally sensitive to environmentally insensitive crack growth occurs at a lower ΔK ($\sim$ 4.5 MPam$^{\frac{1}{2}}$) for R = 0.5 than for R = 0.1 ($\sim$ 7.8 MPam$^{\frac{1}{2}}$) for these constant frequency tests. However, this transition occurs at approximately the same K_{max} value, i.e., $\sim$ 9 MPam$^{\frac{1}{2}}$. This result is consistent with our explanation for the convergence of the H_2O curves with the dry air curves; i.e., as the stress is increased plasticity effects begin to dominate, and environmental effects become less important.

CONCLUSIONS

1. The ΔK_{th} are higher for the T651 condition than for the T7351 condition, regardless of test environment. This is probably due to a higher degree of slip reversibility and more extensive crack branching for the T651 treatment.
2. The crack growth rates are faster for the T7351 condition when compared with the T651 at equivalent ΔK's in dry air. This is related to the more homogeneous deformation and less crack branching of the alloys having the T7351 treatment.
3. An aggressive environment accelerated fatigue crack propagation over that of dry air, for both aging treatments, probably by a form of hydrogen embrittlement.
4. The alloys in the T7351 temper are much less environmentally sensitive than those in the T651 temper.
5. The shape of the growth rate curves can be correlated with a transition in fracture surface appearance which is believed to be controlled by the deformation behavior.

II. STRESS CORROSION CRACKING STUDIES:

High strength aluminum alloys, which are extensively used in aircraft structures, are susceptible to environment-induced subcritical crack growth under sustained stress which is often called stress corrosion cracking (SCC). Considerable effort has been directed towards determining the causes of such failures by examining the microstructure, composition, aging treatment, minor alloy additions, environmental factors and dislocation arrangements but no clear explanation of the stress corrosion fracture process has emerged.

It has been found that the addition of copper to high strength Al-Zn-Mg alloys simultaneously improves the yield strength and stress corrosion cracking resistance.[30-34] An overaging heat treatment may be effectively used to greately enhance stress corrosion resistance without unacceptable strength penalties in copper containing alloys. Inspite of the fact that the impressive beneficial effects of copper addition to Al-Zn-Mg alloys have been known for about a decade, no systematic study has been carried out to clearly establish the role of copper.

This research program was designed to systematically sort out the effects of copper additions on the stress corrosion cracking behavior of 7XXX type high strength Al-Zn-Mg alloys. The four Al-6%Zn-2%Mg-X%Cu alloys described in the previous section and having almost identical microstructures were chosen to study the effect of copper contents on stress corrosion cracking characteristics in a 3.5% NaCl solution. The influence of copper on microstructure, aging kinetics, dislocation structure or deformation mode and electrochemical characteristics were correlated with the SCC kinetics determined by the fracture mechanics method.

EXPERIMENTAL PROCEDURES

In the present set of experiments, short transverse double cantilever beam (DCB) specimens dimensioned to promote a plane strain condition at the crack front, have been used for determining the crack growth rate data as a function of crack tip stress intensity (K_1). The fatigue precracked samples were loaded with opposing bolts to constant crack opening displacement (COD) values. The notch with the precrack was sealed with Scotch tape on both sides of the specimen and the test solution (3.5% NaCl in distilled water) was added to the notch from the top.

RESULTS AND DISCUSSION

Stress corrosion cracking is a stress activated cracking process. In region I, the cracking process is not rate limited when the externally applied stress varies. It is strongly affected by K_1, indicating that the factors that affect the effective local stresses at the crack tip affect the crack growth velocity. The critical local stress necessary for a certain crack growth velocity in region I is provided, in part, by the dislocations piled up at the grain boundary, i.e., $\tau_c = n\tau_{RSS}$ where τ_{RSS} is resolved shear stress and n is the number of dislocations in the pile-up. In the T651 condition, the 0% Cu alloy has an inhomogeneous, planar deformation mode and, therefore, n is very high. So a high stress concentration results at the tip of the pile-up at the high angle grain boundary and the stress corrosion cracking velocity is high, Figure 2. An addition of 1% Cu has no effect on the deformation mode, n remains more or less the same and stage I cracking is not affected, Figure 9. As the amount of copper is increased to 1.6%, region I is shifted to higher stress intensity values. This results from a change in deformation mode from inhomogeneous planar to homogeneous looping which decreases in n and which produces a decreased stress concentration effect. To achieve the minimum stress required for stress corrosion crack propagation, τ_{RSS} has to increased, i.e., the externally applied stress has to be raised. Increasing the copper content to 2.1 shifts region I more to the right by further homogenizing the deformation mode. These observations support the view that region I crack growth is mainly sensitive to mechanical factors.

Increasing the copper content decreases the plateau velocity and this is attributed to the changes in the electrochemical potentials of the phases resulting from the changes in composition. In 7XXX series alloys, the η phase

is anodic with respect to the matrix which is cathodic. If the alloy contains copper, copper goes into the η phase and makes it less anodic. So the potential difference between the cathodic matrix and anodic η phase decreases. This decrease in potential difference would decrease the rate of dissolution of the anodic grain boundary precipitates. The decrease in anodic dissolution is at the same time accompanied by a decrease of hydrogen ion reduction. The copper addition may also affect region II cracking by reducing the rate of transport of hydrogen as the homogeneity of deformation improves. Thus the improvement of the stress corrosion cracking characteristics by the addition of copper can be related to the effects of electrochemical dissolution and the availability and transport of hydrogen.

The improvement in region I of the v-K_1 curve of the 0% Cu alloy by overaging, Figure 10, is attributed to the change in deformation mode from inhomogeneous in the T651 condition to homogeneous in the T7351 condition. Consequently, the stress concentrations at the grain boundaries are reduced. This is reflected in an appreciable shift of region I to higher stress intensities, supporting the view that stage I crack growth rate is affected mainly by mechanical variables. Because of extremely slow crack growth rates, no data of region I has been obtained in any of the copper containing alloys.

The extent of improvement of the region II kinetics by overaging increases with increasing copper content of the alloy, Figures 10 and 11. The crack growth rates for the alloys containing 1.6 and 2.1% copper were too slow to measure (no growth measured in 4 months) in the -T7351 condition. The contribution of copper to the effectiveness of overaging in improving the SCC resistance can be judged from the response of some commerical Al-Zn-Mg-Cu alloys. Copper-containing alloys like 7075 can be made resistant to SCC by

the -T73 overaging treatment. However, for low copper alloys like 7079 a considerable amount of overaging is required, with a corresponding severe strength penalty, for improved SCC resistance. The improvement in SCC resistance by overaging the copper-containing alloys is attributed to a greater amount of copper in η' and η. Enrichment of the precipitates in copper by the overaging treatment has been reported. More copper in η' and η due to overaging makes it even less anodic with respect to the matrix. This further reduces the rates of electrochemical dissolution and/or hydrogen embrittlement.

The reason for the improvement in region II of the copper-free alloy is unclear since no change in chemical composition of the precipitate and matrix is expected with overaging. However, there may be a minor change in electrochemical potential difference between matrix and precipitate associated with the change in crystal structure with overaging, i.e., $\eta' \rightarrow \eta$. In addition, the rate of transport of hydrogen is expected to be reduced as the deformation mode changes from inhomogeneous to homogeneous by overaging. Overaging may also affect the stress corrosion crack growth by resulting in localized changes in the composition of the grain boundary zone.

In the present investigation, the effect of copper on the stress corrosion cracking characteristics of a Al-6%Zn-2%Mg alloy has been studied with all other variables remaining constant. Copper was found to change the deformation mode in the peak strength condition from inhomogeneous planar slip in the copper-free alloy to a homogeneous looping mechanism in the alloys with higher copper contents (1.6%). This mechanical effect, along with the beneficial electrochemical effect of copper, improved the stress corrosion resistance. Overaging treatments also improve the stress corrosion resistance

by affecting the deformation mode and the electrochemical activity of the precipitates.

III. ALLOY DEVELOPMENT IN ALUMINUM-LITHIUM SYSTEMS

Impurity Effects in Al-Li-Alloys: In-situ Auger analysis of fractured Al-Li-Mg alloys have shown the presence of large quantities of sodium, potassium, and sulfur on the fracture surfaces. These elements are probably introduced to the aluminum as impurities in the lithium. Unlike lithium, these elements have virtually no solubility in aluminum. The low solubility of a species such as sodium may lead to unwanted segregation to the grain boundaries promoting intergranular fracture. Consequently, we have had five aluminum-lithium-sodium alloys cast at Alcoa Laboratories. The analyses for these alloys are given in Table 6. These alloys will be forged, and specimens for "in-situ" fracture and Auger analysis of the fracture surfaces will be prepared. This phase of the research is designed to establish a relationship (if any) between the presence of an impurity and the workability and fracture behavior.

Effect of Overaging on the Ductility of Al-Cu-Li (2020): To determine if the ductility of Al-Cu-Li could be regained by overaging 2020-T651, duplicate longitudinal tensile tests were conducted on sample blanks overaged at 250°C for various times up to 24 hours. The average yield strengths and elongations are summarized in Table 7. In general, the yield strength decreased with a concomitant increase in elongation as time at 250°C increased. Specimens for fractographic analysis have been prepared for scanning electron fractography and specimens have been prepared for TEM investigations.

Corrosion Investigation of Al-Li Alloys: This section summarizes the preliminary results of a corrosion investigation conducted on Al-2.8Li-0.3Mn and Al-3.4Li-1.26 Mn sheet. The basic corrosion studies have been completed

and a detailed microstructural investigation of active corrosion sites will be presented. The alloys were solution heat treated at 555°C ± 2C° for 15 minutes, and then cold water quenched. Specimens were isothermally aged at 200°C ± 5C° for .25, 12, 24 and 336 hours.

EXPERIMENTAL PROCEDURES

The following experiments were conducted:

1. Specimen Preparation: All but the corrosion rate specimens were prepared by vacuum casting 1cm X 1cm slices of the different microstructures in epoxy, polishing each to 0.05 microns, and by ultrasonic cleaning prior to testing. The corrosion rate specimens were prepared by abrading 1 cm X 1cm sections of each microstructure on 600 grit SiC paper.
2. Corrosion Potential Measurements: Duplicate specimens from each alloy were immersed in a 3.5% NaCl solution, at room temperature and at a constant stir rate, along with a Standard Calomel Electrode. After 24 hours of immersion the potential differences between the calomel electrode and the specimens were measured and recorded.
3. Dearated Anodic Potentiodynamic Measurements: Deaerated anodic polarization curves were obtained for duplicate specimens of the material artifically aged for 0.25 hour and 336 hours and for single specimens of the material aged for 12 hours and 24 hours. Each curve was obtained by immersing the specimens in a deaerated and agitated 3.5% NaCl electrolyte, and then by driving each specimen as an anode, from potential values more negative (anodic) than their corrosion potentials to values slightly more positive (cathodic) than their breakdown potentials. The solutions were deaerated by bubbling N_2 through the test cell for 1 hour prior to and during each scan. The potentials were increased at a constant scan

rate of 10 mV/min (in accordance with ASTM G5) and were recorded along with the resulting current.

4. Deaerated Potentiostatic Measurements: Specimens in the under and over-aged condition were immersed in a deareated and agitated 3.5% NaCl solution. The specimens were maintained at appra corrosion potential for 24 hours and their current density was recorded as a function of time.
5. Corrosion Rate Determination: Specimens of the different microstructures were immersed in aerated and agitated 3.5% NaCl solution for 100 hours. The corrosion rate was determined in accordance with ASTM G1.
6. Metallography: Surface and cross sections were examined metallographically from selected corrosion specimens to determine the type and degree of attack.

RESULTS

The results of the corrosion investigation are summarized in Table 8 and the accompanying graphs and photomicrographs are presented in Figures 12-20.

DISCUSSION OF THE RESULTS

It is evident from the results of each of the corrosion experiments conducted (Table 8) that increases in both manganese content and isothermal aging time, have a deleterious effect on the corrosion behavior of precipitation hardening Al-Li alloys in a 3.5% NaCl solution. The changes in the susceptibility of the two Al-Li alloys with aging and mangenese content can be correlated to specific microstructural features.

The controlled microstructure variables in this investigation were the volume fraction of secondary intermetallic particles and despersoids, the size and distribution of metastable Al_3Li (δ') precipitates, and the grain size. Each of these microstructure variables have an effect on the corrosion behavior of these alloys.

The secondary intermetallic particles (coarse intermetallics which form during eutectic decomposition of the liquid solution) and the disperoids, (intermetallics which form by solid state precipitation during ingot preheat) create a galvanic couple between themselves and the matrix. This galvanic couple is the result of the potential difference that exists between the particles and the matrix. Increasing the amount of Mn increases the volume fraction of both the secondary intermetallics and dispersoids, as shown in Figure 12, and thereby increases the propensity for galvanic action. Figure 13 shows the surface corrosion after 48 hours of exposure. The presence of intermetalics is partly responsible for the severity of the attack. Increasing the volume fraction of these particles increases the attack.

Numerous investigations have shown that δ' develops in Al-Li by homogeneous decomposition upon quenching from the solution heat treatment temperatures. The growth process follows a $(\text{time})^{1/3}$ dependence, along with the growth of the matrix precipitates, preferential coarsening of precipitates near grain boundaries occurs. To accommodate the accelerated growth in the grain boundary regions, a precipitate free zone (PFZ) develops, the change in the width of the PFZ has also been shown to occur at a rate proportional to $(\text{time})^{1/3}$. Evidence of the PFZ development and growth of the matrix precipitates are shown in Figure 16. These changes in size and distribution of δ' affect the corrosion behavior. A galvanic couple forms between the anodic grain boundaries and intermetallic-matrix interfaces and the cathodic, solute depleted, PFZ. Figures 17 and 18 show the increase in grain boundary and particle attack resulting from the changes in size and distribution of δ'.

Tenatively two conclusions can be drawn from this research.

1. Overaging has a deleterious effect on the succeptibility of attack of Al-Li alloys in 3.5% NaCl, and
2. increasing the volume fraction of mangenese containing phases, also increases the susceptibility of attack.

To further understand the mechanisms of attack in Al-Li alloys, we are planning to investigate the effect of volume fraction of δ' on the corrosion process by studying three binary Al-Li alloys having the nominal compositions, 1, 2 and 3 weight per cent lithium. Furthermore, we plan to evaluate chronium as an alternate alloying element to replace manganese.

The Effect of Dispersoids on the Homogenization of Slip in 2020: Homogenization of tensile deformation can be accomplished by either refining the grain size or by introducing non-shearable precipitates. The alloy 2020 contains approximately 0.5 weight percent manganese. Manganese forms the incoherent $Al_{20}Mn_3Cu_2$ precipitate in Al-Cu-Li during high temperature (516°C) ingot preheating. These precipitates are rod-like and are on the order of 0.1 μm long by 0.05 μm in diameter. An investigation is being conducted with Dr. A. K. Vasuedauan of Alcoa Laboratories. The purpose is to explore the interaction of artifical aging precipitates and slip distribution on the fracture behavior of 2020.

Tensile blanks of 2020 were aged at 135° and 160°C. Tensile tests were conducted and TEM investigations were conducted on thin sections prepared from below the aged fractured specimens. When the alloy was aged at 135°C the maximum yield strength was low (210 MPa) but the elongation was high (20%); however, aging at 160°C resulted in a large maximum yield strength (530 MPa) but a low elongation (5%). The TEM results, Figure 21, showed that the deformation structure could be correlated with the fracture mode. When the failure was

transgranular, the slip distance was modified by the manganese dispersoids. On the other hand, aging to maximum strength resulted in intergranular failure and slip bands were observed to traverse the grains and terminate at grain boundaries. Thus, for the given volume fraction and distribution of manganese in 2020, the influence of the manganese precipitates diminished with increased strength. However, these results suggest that it may be fruitful to investigate the effects of increasing the volume fraction of the small manganese dispersoids in order to maintain the dispersoid controlled slip length to higher strengths.

PROFESSIONAL PERSONNEL

Dr. Edgar A. Starke, Jr.
Dr. Thomas H. Sanders, Jr.
Dr. Saghana B. Chakrabortty
Dr. Fu-Shiong Lin

GRADUATE STUDENTS

B. Sarkar
Charles Heikkenen
Paul Niskanen

DEGREES GRANTED UNDER AFOSR SPONSORSHIP

AFOSR-71-2064

Billy R. Livesay, "Dislocation Interactions at Interfaces," Doctor of Philosophy, March, 1972.

Saghana B. Chakrabortty, "Deformation Twinning in Cu_3Au," Doctor of Philosophy, Janaury, 1974.

Kuang-Ho Chien, "The Effect of Ordering on Low Cycle Fatigue of Cu_3Au, " Doctor of Philosophy, September, 1974.

AFOSR-74-2615

Thomas H. Sanders, Jr., "The Relationship of Microstructure to Monotonic and Cyclic Straining in Two Aluminum-Zinc-Magnesium Precipitation Hardening Alloys," Doctor of Philosophy, February, 1975.

Edmund Jung Chen, "Effects of Ion-Plating on Low Cycle Fatigue Behavior of Copper Single Crystals," Doctor of Philosphy, July, 1975.

Robert E. Sanders, Jr., "The Effect of Zirconium on the Low Cycle Fatigue Behavior of an Aluminum-Zinc-Magnesium Alloy," Master of Science, June, 1976.

Edward J. Coyne, Jr., "The Effect of Microstructure on the Fatigue Crack Propagation Behavior of an Aluminum-Zinc-Magnesium-Zirconium Alloy," Master of Science, March, 1977.

AFOSR-78-3471

Fu-Shiong Lin, "Low Cycle Corrosion Fatigue and Crack Propagation of High Strength 7XXX-Type Aluminum Alloys," Doctor of Philosophy, April, 1978.

Bhaskar Sarkar, "Stress Corrosion Characteristics of Al-Zn-Mg Alloys with Copper Additions," Doctor of Philosophy, August, 1979.

PUBLICATIONS UNDER AFOSR SPONSORSHIP

AFOSR-71-2064

1. B. R. Livesay and E. A. Starke, Jr., "Interactions of Dislocations with Interfaces," Acta. Met., 21 (1973) pp. 247-254.

2. S. B. Chakrabortty and E. A. Starke, Jr., "Deformation Twinning of Cu_3Au," Acta Met., 23 (1975) pp. 63-71.

3. K. H. Chien and E. A. Starke, Jr., "The Effect of Order on the Low Cycle Fatigue Response of Cu_3Au Single Crystals," Acta Met. 23, 1173-1184 (1975).

4. E. Y. Chen and E. A. Starke, Jr., "Effects of Ion-Plating on Low Cycle Fatigue Behavior of Copper Single Crystals," Mater. Sci. and Engr., 24, No. 2, 209-221 (1976).

AFOSR-74-2615

5. T. H. B. Sanders and E. A. Starke, Jr., "The Effects of Microstructural Features on the Response of Aluminum Alloys to Cyclic Deformation," Met. Trans., 7A, 1407-1418 (1976).

6. M. Marek and E. A. Starke, Jr., "Potential Distributions Relating to Grain Boundaries on Corroding Aluminum Alloys," Br. Corros. J., 11, 31-34 (1976).

7. R. E. Sanders, Jr., and E. A. Starke, Jr., "The Effect of Grain Refinement by Al_3Zr on the Low Cycle Fatigue Behavior of an Aluminum-Zinc-Magnesium Alloy," Mater. Sci. and Engr., 28, No. 1, 53-68 (1977).

8. Fu-Shiong Lin and E. A. Starke, Jr., "Low Cycle Corrosion Fatigue of an Al-Zn-Mg-(Zr) Alloy," Fracture 1977, 2, 879-885, Waterloo, Canada, June 19-24, 1977.

9. E. J. Coyne, Jr. and E. A. Starke, Jr., "The Effect of Microstructure on the Fatigue Crack Growth Behavior of an Al-Zn-Mg-(Zr) Alloy," Inter. J. of Fracture, 15, 405-417 (1979).

AFOSR-78-3471

10. Fu-Shiong Lin and E. A. Starke, Jr., "The Effect of Copper Content and Degree of Recrystallization on the Fatigue Resistance of 7XXX Type Aluminum Alloys, I. Low Cycle Corrosion Fatigue," Mater. Sci. and Engr., 39, 27-41 (1979).

11. E. E. Underwood and E. A. Starke, Jr. "Quantitative Stereological Methods for Analyzing Important Microstructural Features in Fatigue of Metals and Alloys," in STP 675, ASTM, Philadelphia, PA (1979) pp. 633-682.

12. Fu-Shiong Lin and E. A. Starke, Jr., "The Effect of Copper Content and Degree of Recrystallization on the Fatigue Resistance of 7XXX-Type Aluminum Alloys, II. Fatigue Crack Propagation," Mater. Sci. and Engr., 43, No. 1, 65-76, (1980).

13. Fu-Shiong Lin and E. A. Starke, Jr., "The Effect of Copper Content and Deformation Mode on the Corrosion Fatigue Crack Growth Behavior of Al-6Zn 2Mg-XCu Alloys at Low Stress Intensities," Mater. Sci. Engr. (in press).

Respectfully submitted:

Edgar A. Starke, Jr.

Edgar A. Starke, Jr.
Principal Investigator

REFERENCES

1. P. C. Paris and F. Erdogan, J. Basic Eng., Vol. 85, 1963, p. 528.
2. R. O. Ritchie, Metal Science, Vol. 11, 1977, p. 368.
3. C. J. Beevers, ibid, Vol. 11, 1977, p. 362.
4. C. J. Beevers, Fracture 1977 , Vol. 1, 1CF4, 1977.
5. M. V. Hyatt and W. E. Quist, Technical Report AFML-TR-67-329, 1967, p. 827.
6. M. O. Speidel, NATO Advanced Study Institute on SCC, Copenhagen, Denmark, July, 1975.
7. R. M. N. Pelloux, Fracture, Proc. of the Second Int. Conf. on Fracture, Brighton, 1969, p. 731.
8. A. R. Rosenfield, C. W. Price and C. J. Martin, Research on Synthesis of High-Strength Al Alloys, Part II, AFML-TR-74-129, 1972.
9. S. M. El-Soudani and R. M. N. Pelloux, Met. Trans., Vol. 4, 1973, p. 171.
10. J. A. Feeney, J. C. McMillan and R. P. Wei, Met. Trans., Vol. 1, p. 1741.
11. W. G. Truckner, J. T. Staley, R. J. Bucci and A. B. Thakkern, "Effect of Microstructure on Fatigue Crack Growth of High Strength Aluminum Alloys," AFML-TR-76-169, May, 1976.
12. Fu-Shiong Lin and E. A. Starke, Jr., Mat. Sci. & Eng., 39 (1979) p. 27.
13. W. G. Clark, Jr., and S. J. Hudak, Jr., J. Test Eval., 3, (1975) p.454.
14. A. J. Sedriks, J. A. S. Green and D. L. Novak, Corrosion-NACE, Vol. 27, (1971), p. 198.
15. Edgar A. Starke, Jr. and Gerd Lütjering, in Fatigue and Microstructure, American Society for Metals, Metals Park, Ohio, 1979, p. 205.
16. E. A. Starke, Jr., Mat. Sci. & Eng., 29, 1977, p. 99
17. Fu-Shiong Lin and E. A. Starke, Jr., "The Effect of Copper Content and Degree of Recrystallization on the Fatigue Resistance of 7XXX-Type Aluminum Alloys, II. Fatigue Crack Propagation," Mater. Sci. and Engr. (in press).
18. T. L. MacKay, Engr. Frac. Mech., Vol. 11, (4), 1979, p. 753.
19. R. W. Hertzberg and W. J. Mills, ASTM STP 600, 1976, p. 220.
20. S. B. Chakrabortty and E. A. Starke, Jr., "Fatigue Crack Propagation of Metastable Beta Titanium-Vanadium Alloys," Met. Trans. A., (in press).

21. C. Laird and G. C. Smith, Phil. Mag., 7, 1962, p. 847.

22. C. Laird and de la Veux, Met. Trans. A., 8A, 1977, p. 657.

23. J. Lindigkeit, G. Terlinde, A. Gysler, and G. Lütjering, Acta Met., 27, (1979) p. 1717.

24. A. Gysler, J. Lindigkeit, and G. Lütjering, Proceedings of the 5th International Conference on the Strength of Metals and Alloys, Aacher, Germany, (1979) 2, p. 1113.

25. J. Petit, B. Bouchit, C. Goss and J. deFouguet, Fracture 1977, ICF4, 2, Waterloo, Canada, 1977, p. 867.

26. B. W. Lifta and D. O. Sprowls, ASTM-ST- 516, Philadelphia, PA, 1972, p. 120.

27. Richard W. Hertzberg, Deformation and Fracture Mechanics of Engineering Materials, John Wiley and Sons, New York, 1976.

28. R. Jacko and D. T. Duquette, Met. Trans. A, (1977), p. 1821.

29. C. J. Beevers, Fracture 1977, ICF4, 1, Waterloo, Canada, 1977, p. 239.

30. M. O. Speidel, Current Understanding of Stress Corrosion Crack Growth in Al Alloys, NATO Science Committee Research Evaluation Conference, Brussels (1971).

31. M. O. Speidel, Met. Trans., Vol 6A, 631, (1975).

32. M. O. Speidel and M. V. Hyatt, Advances in Corrosion Science and Technology, Vol 2, Plenum Press (1972).

33. J. T. Staley, H. Y. Hunsicker and R. Schmidt, AIME-TMS, paper F 71-7, (1971).

34. M. V. Hyatt and M. O. Speidel--High Strength Al Alloys--in "SCC in High Strength Steels and Al Alloys"--Ed. B. F. Brown NRL, Washington, D.C. (1972).

LIST OF TABLES

TABLE 1. CHEMICAL COMPOSITION (WEIGHT PERCENT) OF THE FOUR ALUMINUM ALLOYS

Alloy	Cu	Zn	Mg	Zr	Ti	Fe	Si	Al
0.0 Cu	0.01	6.41	2.08	0.11	0.02	0.05	0.05	bal.
1.0 Cu	0.98	6.10	2.20	0.12	0.02	0.05	0.05	bal.
1.6 Cu	1.56	6.07	2.24	0.12	0.02	0.05	0.06	bal.
2.1 Cu	2.11	5.97	2.11	0.12	0.02	0.07	0.06	bal.

TABLE 2

MICROSTRUCTURAL PARAMETERS AND MONOTONIC PROPERTIES

ALLOY	VOLUME PERCENT RECRYSTALLIZED	SUBGRAIN SIZE (μm)	UNRECRYSTALLIZED GRAIN SIZE (μm)	YIELD STRENGTH (MPa) T651*	YIELD STRENGTH (MPa) T7351	TENSILE STRENGTH (MPa) T651*	TENSILE STRENGTH (MPa) T7351	DUCTILITY (% REDUCTION IN AREA) T651*	DUCTILITY (% REDUCTION IN AREA) T7351	STRAIN HARDENING EXPONENT n T651*	STRAIN HARDENING EXPONENT n T7351	FRACTURE TOUGHNESS K_{IC} MPa$\sqrt{m}$ T651**	FRACTURE TOUGHNESS K_{IC} MPa$\sqrt{m}$ T7351**
0.0 Cu	5	5	1100	482	404	552	440	31	46	.028	0.038	31	36
1.0 Cu	7	4	1100	522	432	558	483	33	41	.031	0.040	32	35
1.6 Cu	9	5	1100	529	463	614	511	33	39	.033	0.049	31	[illegible]
2.1 Cu	12	5	1100	540	430	614	484	35	39	.032	0.047	27	32

*From Lin & Starke, Reference 12

**From B. Sarkar, M. Marek, and E. A. Starke, Jr., unpublished research.

TABLE 3. THRESHOLD ΔK TAKEN AT $da/dN = 1X10^{-10}$ m/cycle FOR DRY AIR AND H_2O FCP TESTS

ALLOY	PEAK-AGED T651		OVER-AGED T7351	
	DRY AIR	H_2O	DRY AIR	H_2O
	$MPam^{\frac{1}{2}}$		$MPam^{\frac{1}{2}}$	
0.01 Cu	---	---	2.6	2.3
1.0 Cu	3.0	2.4	2.6	1.8
1.6 Cu	---	---	2.6	2.0
2.1 Cu	---	---	2.6	2.0

TABLE 4. THE RATIO OF THE FCGR IN DISTILLED WATER TO THAT IN DRY AIR, AT $\Delta K = 7$ MPam$^{\frac{1}{2}}$

ALLOY	$(da/dN)_{H_2O}/(da/dN)_{dry\ air}$	
	PEAK-AGED T651	OVER-AGED T7351
0.0 Cu	50	7
1.0 Cu	39	8
1.6 Cu	14	6
2.1 Cu	13	5

TABLE 5. PARAMETERS OF da/dN-ΔK CURVES FOR THE T7351 CONDITION TESTED IN H_2O

ALLOY	ΔK ($MPam^{\frac{1}{2}}$) of Break Point	SLOPE Below Break	SLOPE Above Break
0.0 Cu	9.0	5.8	3.0
1.0 Cu	8.0	5.0	2.4
1.6 Cu	7.5	4.8	2.6
2.1 Cu	6.5	4.4	2.4

TABLE 6. COMPOSITIONS OF Al-Li-Na ALLOYS

ALLOY	Li	Na	Si	Fe	Al
501036A	3.40	0.001	0.018	0.094	Balance
501037A	3.20	0.022	0.017	0.074	
501038A	3.24	0.034	0.016	0.038	
501039A	3.20	0.070	0.017	0.049	
501040A	3.32	0.080	0.017	0.035	

TABLE 7. THE EFFECT OF OVERAGING AT 250°C ON THE YIELD STRENGTH AND ELONGATION OF 2020

TIME AT 250°C (HOURS)	YIELD STRENGTH (MPa) (0.2% OFFSET)	ELONGATION (%)
0 (T651 condition)	533	5.0
.25	512	8.0
.50	387	10.0
.75	304	10.2
1.0	228	10.75
2.0	224	12.0
2.5	225	10.5
3.0	224	11.0
5.0	216	12.0
8.0	207	12.75
24.0	176	13.5

TABLE 8. CORROSION DATA FOR Al-Li ALLOYS

ALLOY (A)	AGING TIME (HOURS)	CORROSION POTENTIAL (V_{SCE}) (B)	BREAKDOWN POTENTIAL (V)	PASSIVE CURRENT DENSITY (A/cm^2)	POTENTIOSTATIC CURRENT (A/cm^2)	CORROSION RATE mm /YEAR)
ALLOY I	0.25	-0.769	-0.693 (B)	$4.5X10^{-6}$(B)	$1.5X10^{-6}$	0.53
	12.0	-0.780	-0.705	$3X10^{-6}$	(C)	0.48
	24.0	-0.734	-0.720	$1X10^{-6}$	(C)	0.44
	336.0	-1.291	-0.736 (B)	$10X10^{-6}$ (B)	$2.4X10^{-6}$	0.68
ALLOY II	0.25	-0.739	-0.716 (B)	$2X10^{-6}$	$4.8X10^{-6}$	0.47
	12.0	-0.790	-0.780	$9X10^{-6}$	(C)	0.43
	24.0	-1.128	-0.790	$13X10^{-6}$	(C)	0.44
	336.0	-1.326	-0.755 (B)	$145X10^{-6}$ (B)	$124X10^{-6}$	0.95

(A) Alloy Composition
Alloy I - 2.78 Li, 0.32 Mn
Alloy II - 3.43 Li, 1.26 Mn

(B) Average of Two Tests

(C) Not Determined

LIST OF FIGURES

Figure 13. Surface sections of (a) under and (b) overaged specimens after 48 hours in a 3.5% NaCl solution.

Figure 14. Precipitate radius as a function of isothermal aging time. (Anodized, Polarized light).

Figure 15. Illustrating the growth of δ' as a function of aging time at 200°C, (a) 0.25 (b) 12 (c) 24 and (d) 336 hours.

Figure 16. Representative TEMS showing the development of precipitate free zones of low Mn alloy (a) aged at 0.25 hours, and (b) 336 hours.

Figure 17. Optical photomicrographs of the surface of the potentiodynamic anodic polarization specimens, in the (a) under and (b) overaged condition, 1 minute after reaching the breakdown potential. (low Mn alloy)

Figure 18. SEM showing the attack after 48 hours in 3.5% NaCl solution at the interface of the secondary intermetallics. (alloy 2, aged 24 hours)

Figure 19. 3 D photomicrograph showing the grain morphology of Alloy 1. (Anodized, polarized light)

Figure 20. 3 D photomicrograph showing the grain morphology of Alloy 2. (Anodized, polarized light)

Figure 21. (a) When the slip length was controlled by the manganese dispersoids, the failure was transgranular, (b) however, if the slip bands traversed the grain, the failure was intergranular.

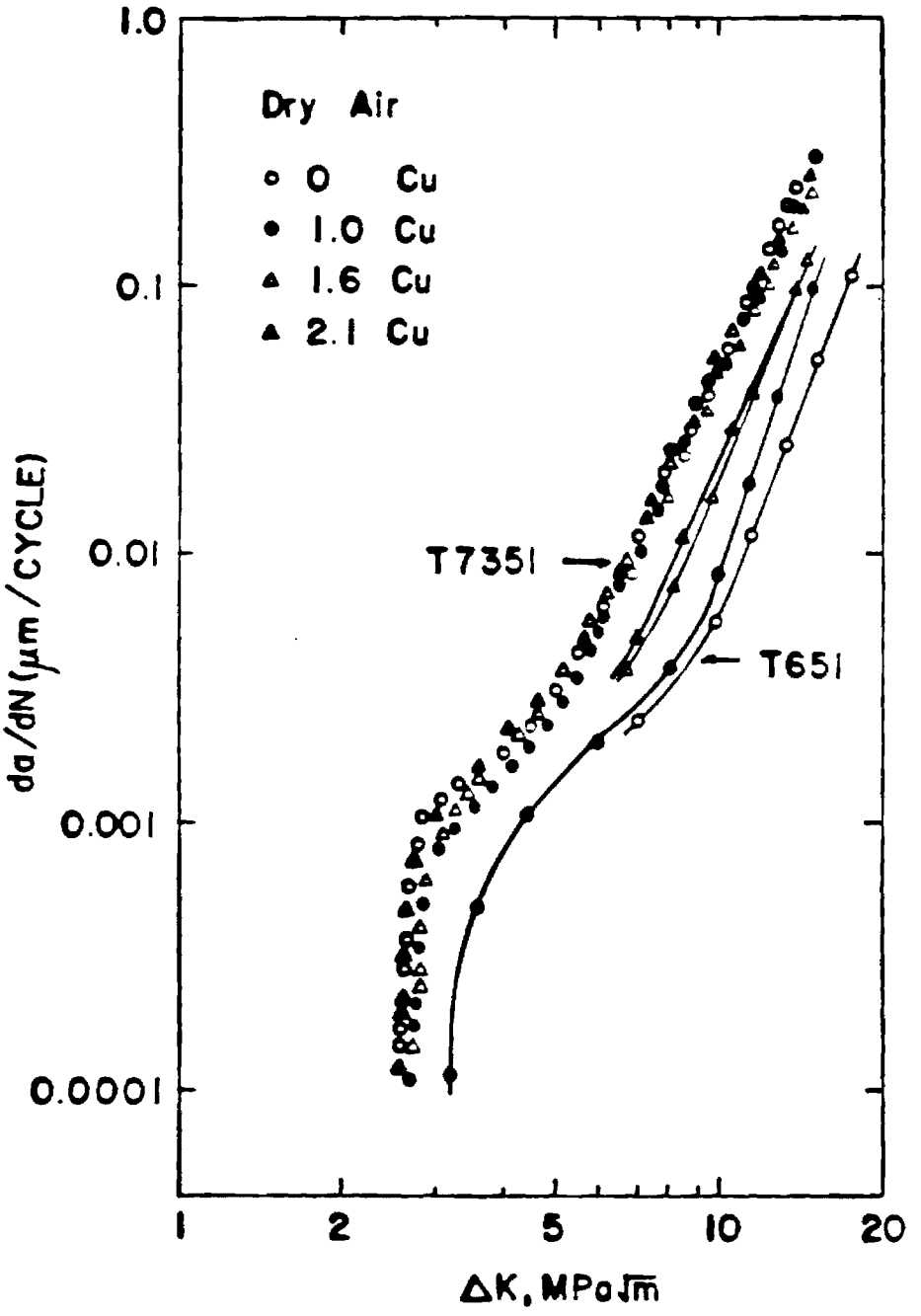

Figure 1. Effect of aging treatment and copper content on the FCGR in dry air.

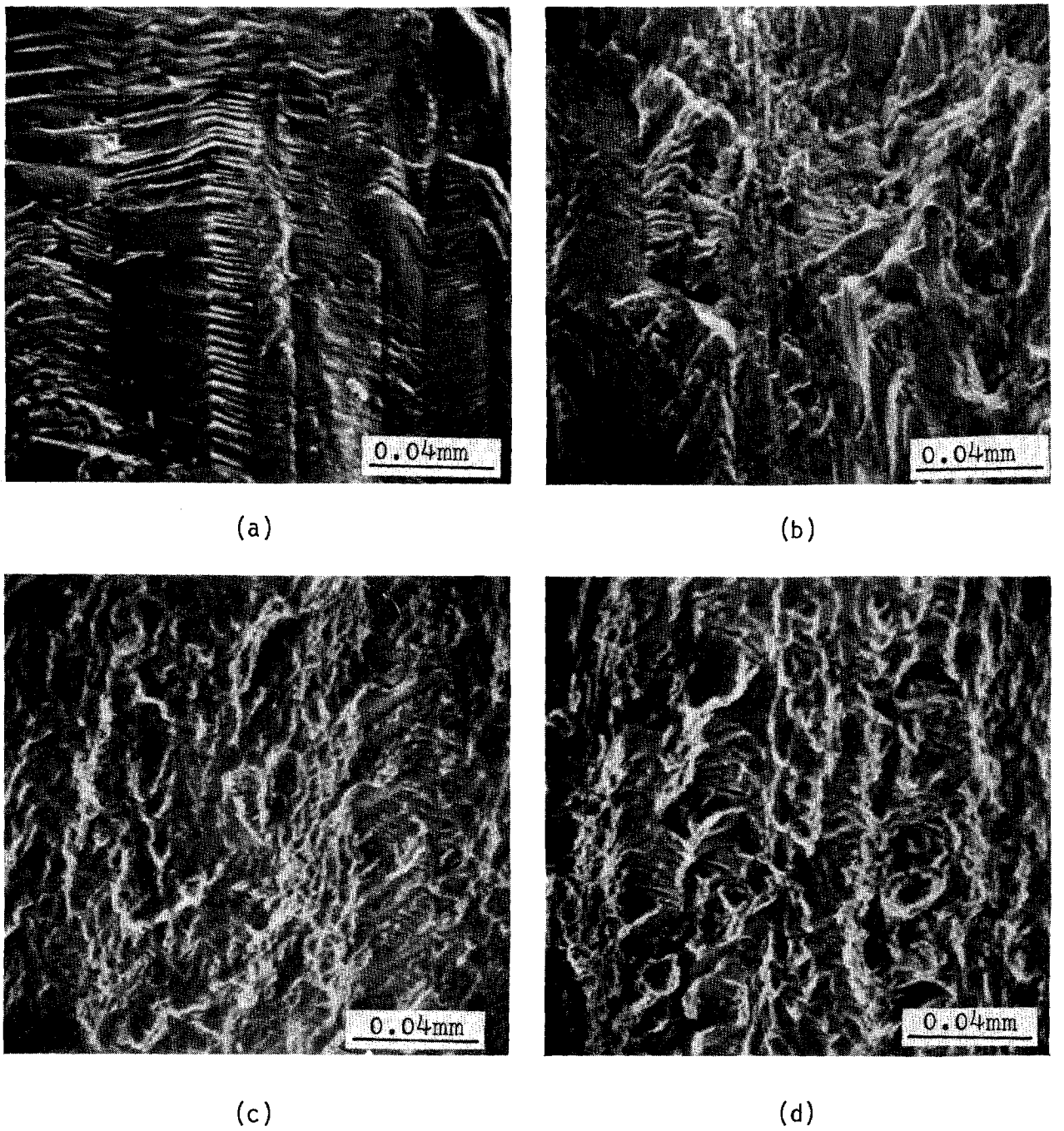

Figure 2. Scanning electron micrographs of the FCP fracture surface for the 1.0% Cu alloy (T7351) tested in dry air, (a) close to the ΔK_{th} value, 2.7 $MPam^{\frac{1}{2}}$, (b) within the bump region, ΔK = 3.6 $MPam^{\frac{1}{2}}$, (c) in Regime II, ΔK = 6.5 $MPam^{\frac{1}{2}}$, and (d) in Regime II, ΔK = 9 $MPam^{\frac{1}{2}}$.

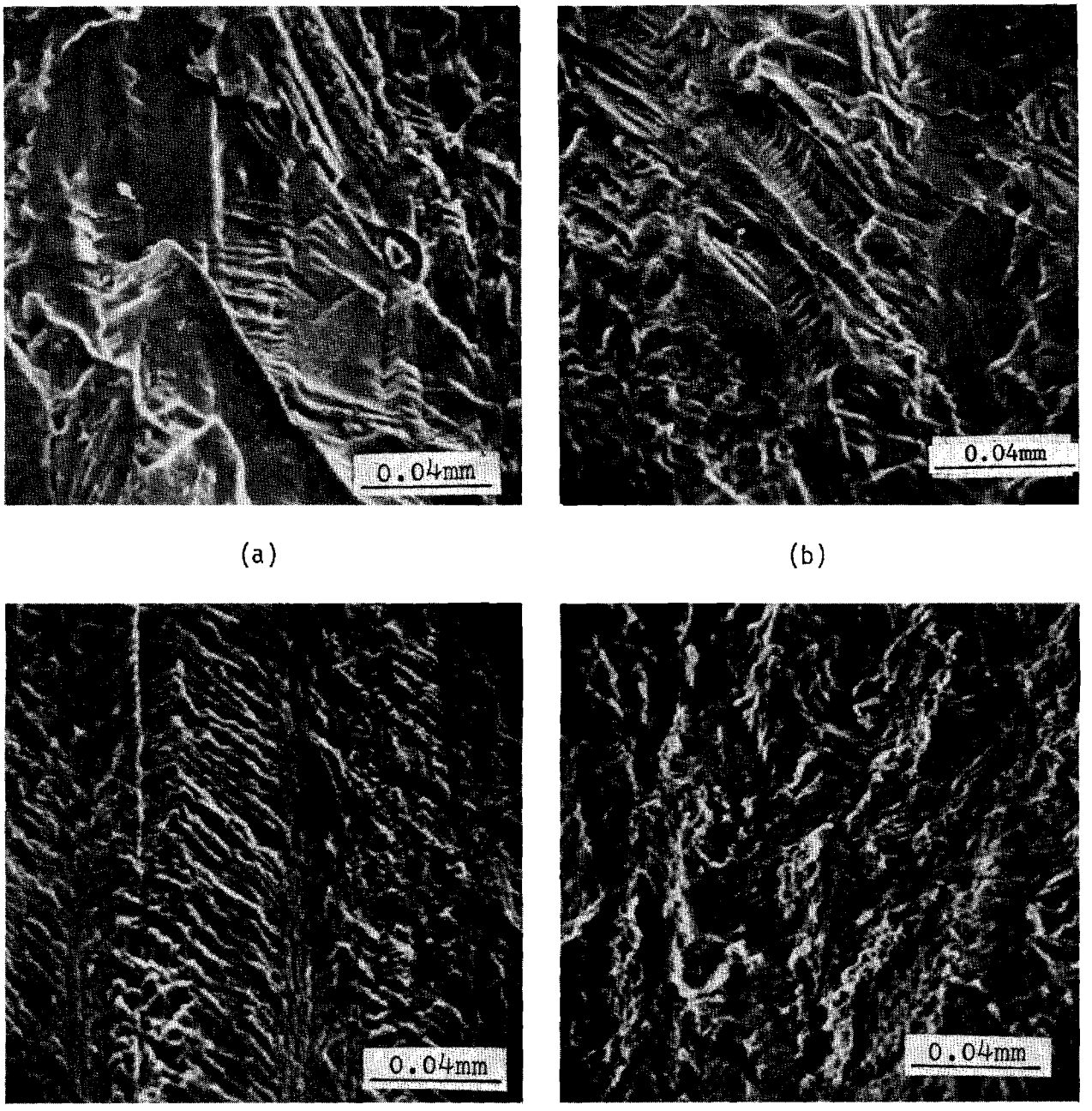

Figure 3. Scanning electron micrographs of the FCP fracture surface for the 1.0% Cu alloy (T651) tested in dry air. (a) close to the ΔK_{th} value, 3.2 $MPam^{\frac{1}{2}}$ (b) within the bump region, ΔK = 5 $MPam^{\frac{1}{2}}$, (c) in Regime II, ΔK = 8 $MPam^{\frac{1}{2}}$, and (d) in Regime II, ΔK = 12 $MPam^{\frac{1}{2}}$.

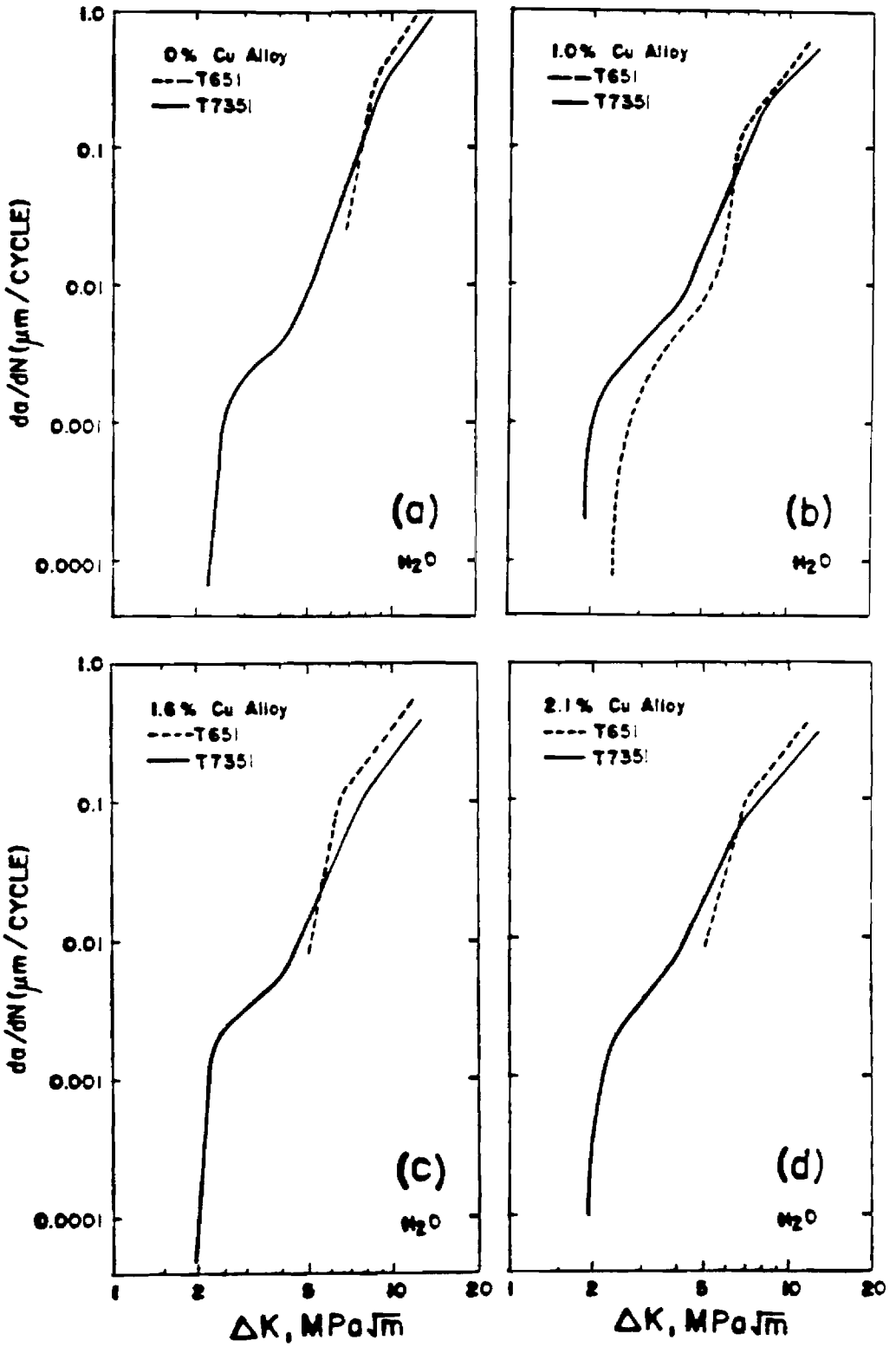

Figure 4. Effect of aging treatment and copper content on the FCGR in distilled water. (a) 0.0% Cu alloy. (b) 1.0% Cu alloy, (c) 1.6% Cu alloy and (d) 2.1% Cu alloy.

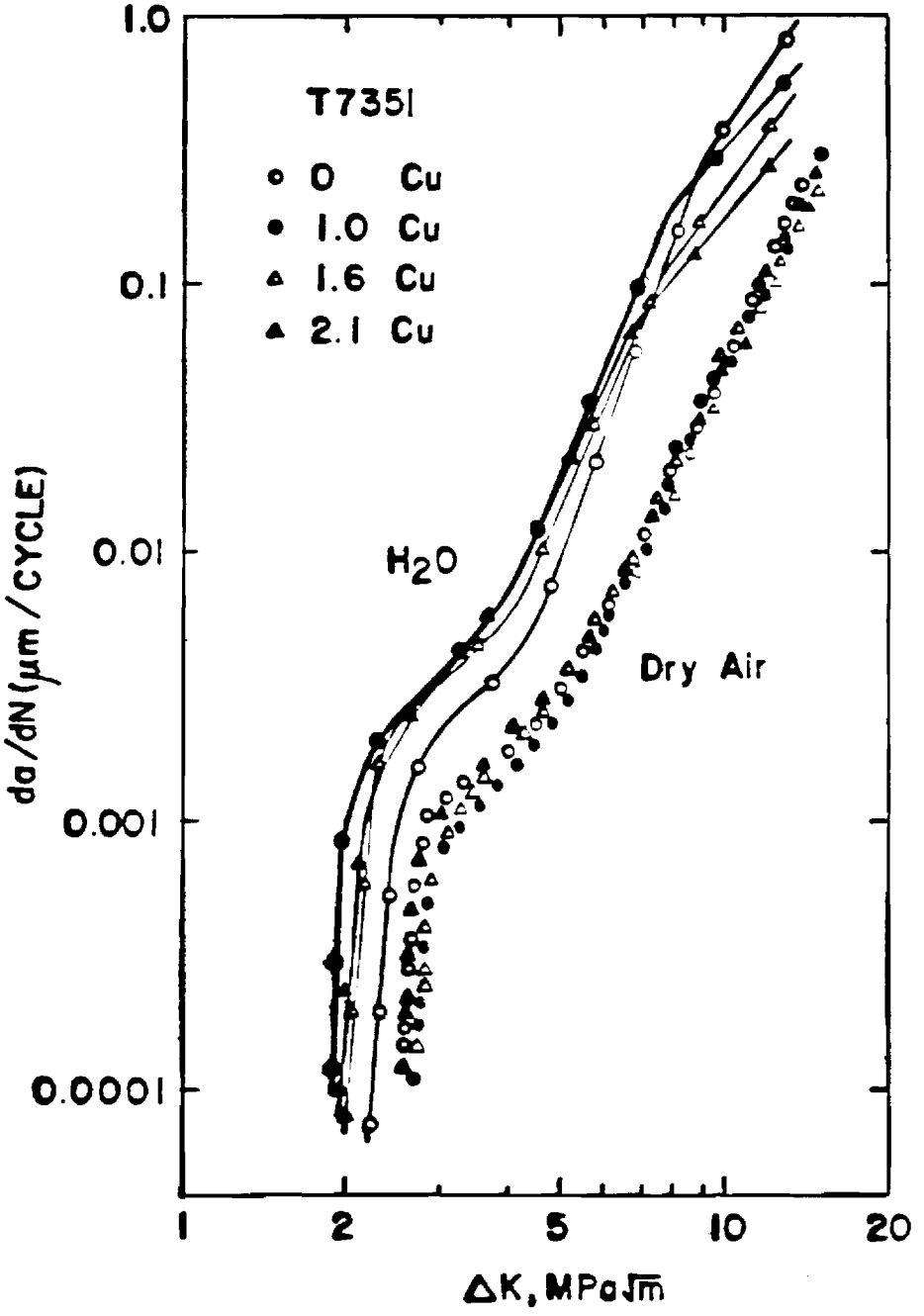

Figure 5. Effect of environment on the FCGR of the alloys in the T7351 condition.

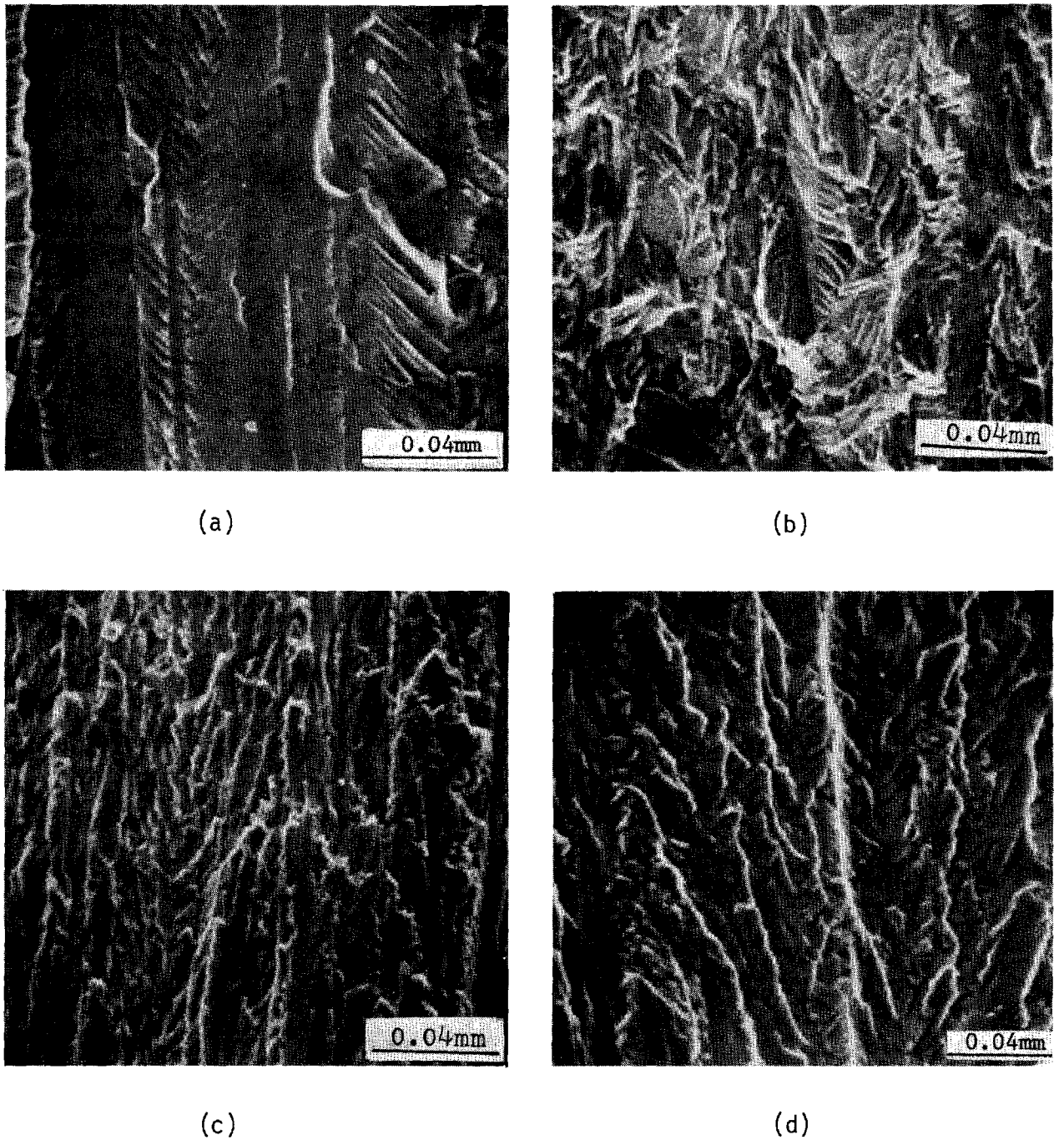

Figure 6. Scanning electron micrographs of the FCP fracture surface for the 1.0% Cu alloy (T7351) tested in distilled water, (a) close to the ΔK_{th} value, 1.9 MPam$^{1/2}$, (b) within the bump region, ΔK = 3 MPam$^{1/2}$. (c) in Regime II, ΔK = 6 MPam$^{1/2}$, and (d) in Regime II, ΔK = 9 MPam$^{1/2}$.

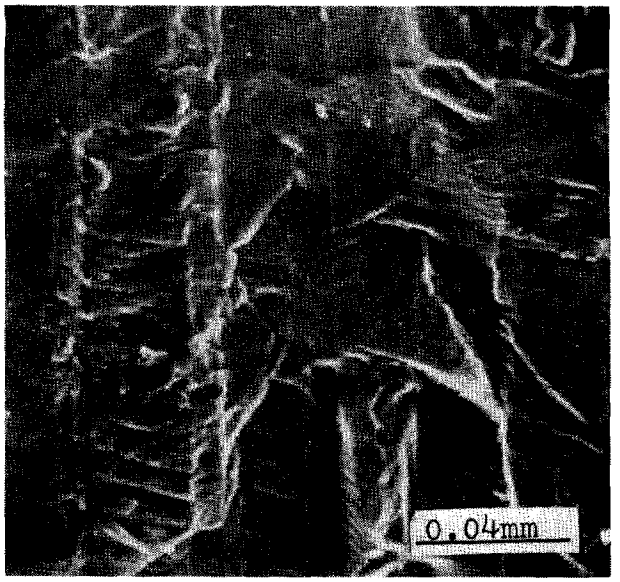

(a)

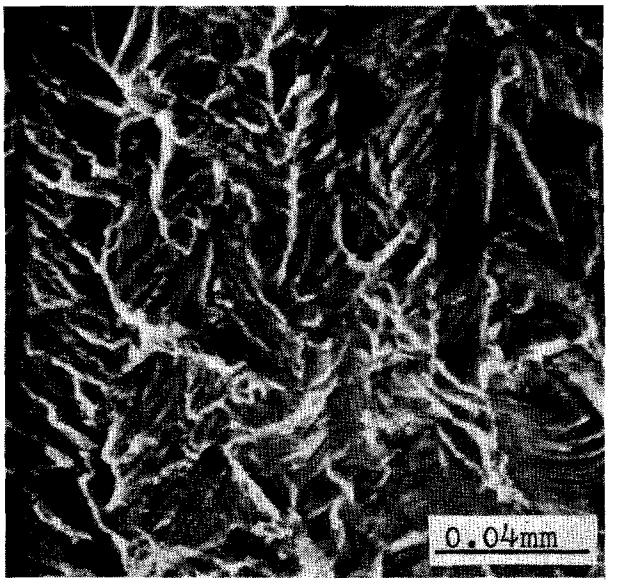

(b)

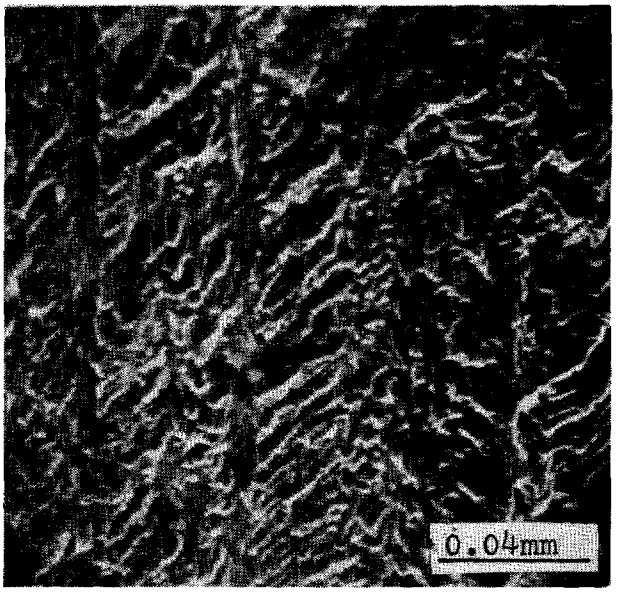

(c)

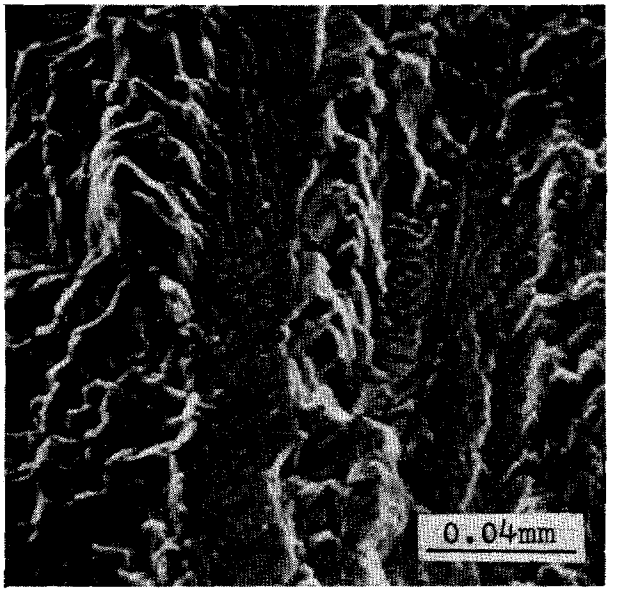

(d)

Figure 7. Scanning electron micrographs of the FCP fracture surface for the 1.0% Cu alloy (T651) tested in distilled water, (a) close to the ΔK_{th} value, 2.4 MPam$^{1/2}$, (b) in the bump region, ΔK = 4 MPam$^{1/2}$, (c) in Regime II, ΔK = 6 MPam$^{1/2}$ and (d) in Regime II, ΔK = 9 MPam$^{1/2}$.

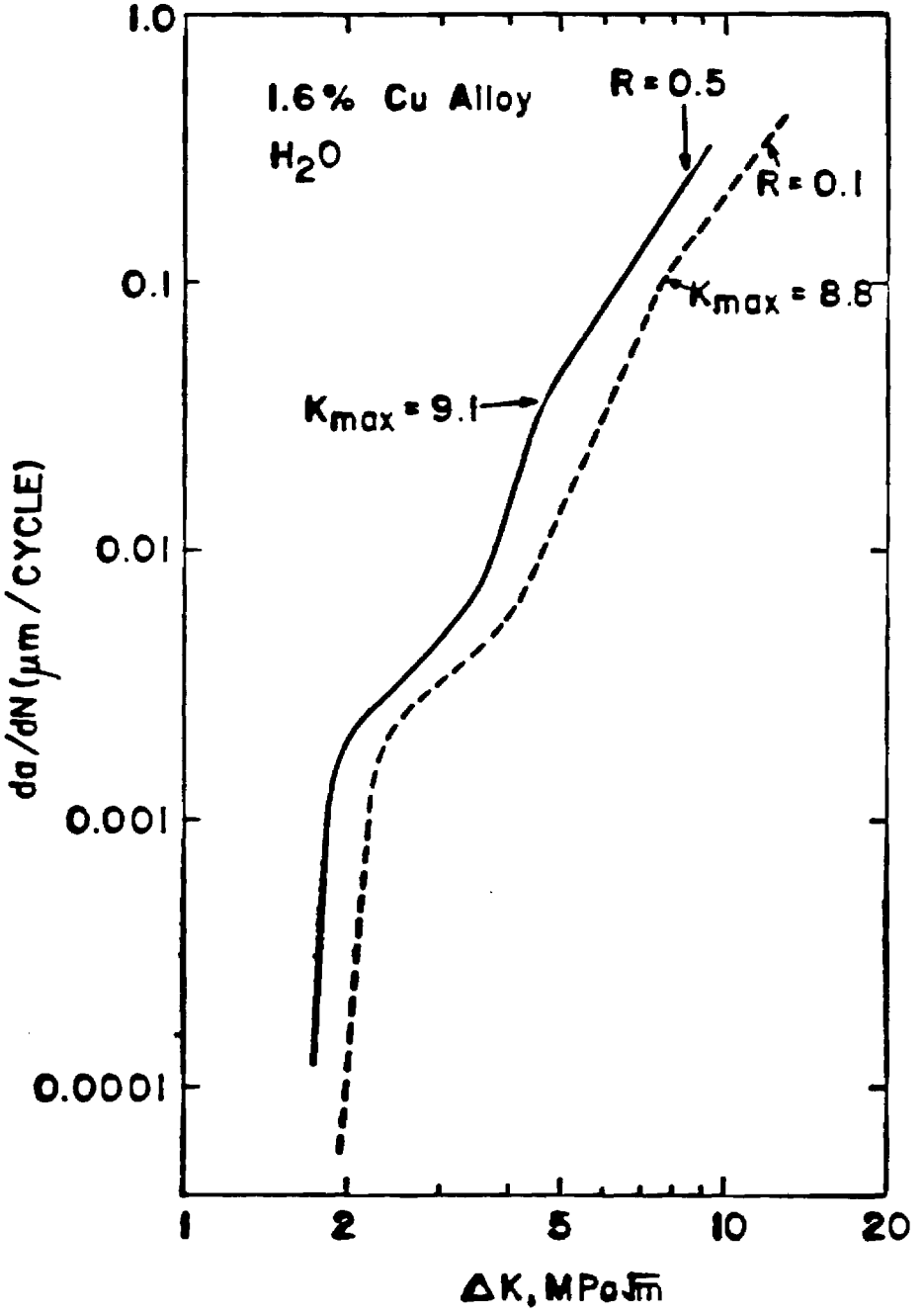

Figure 8. Effect of R ratio on the FCGR of the 1.6% Cu alloy in the T7351 condition tested in distilled water.

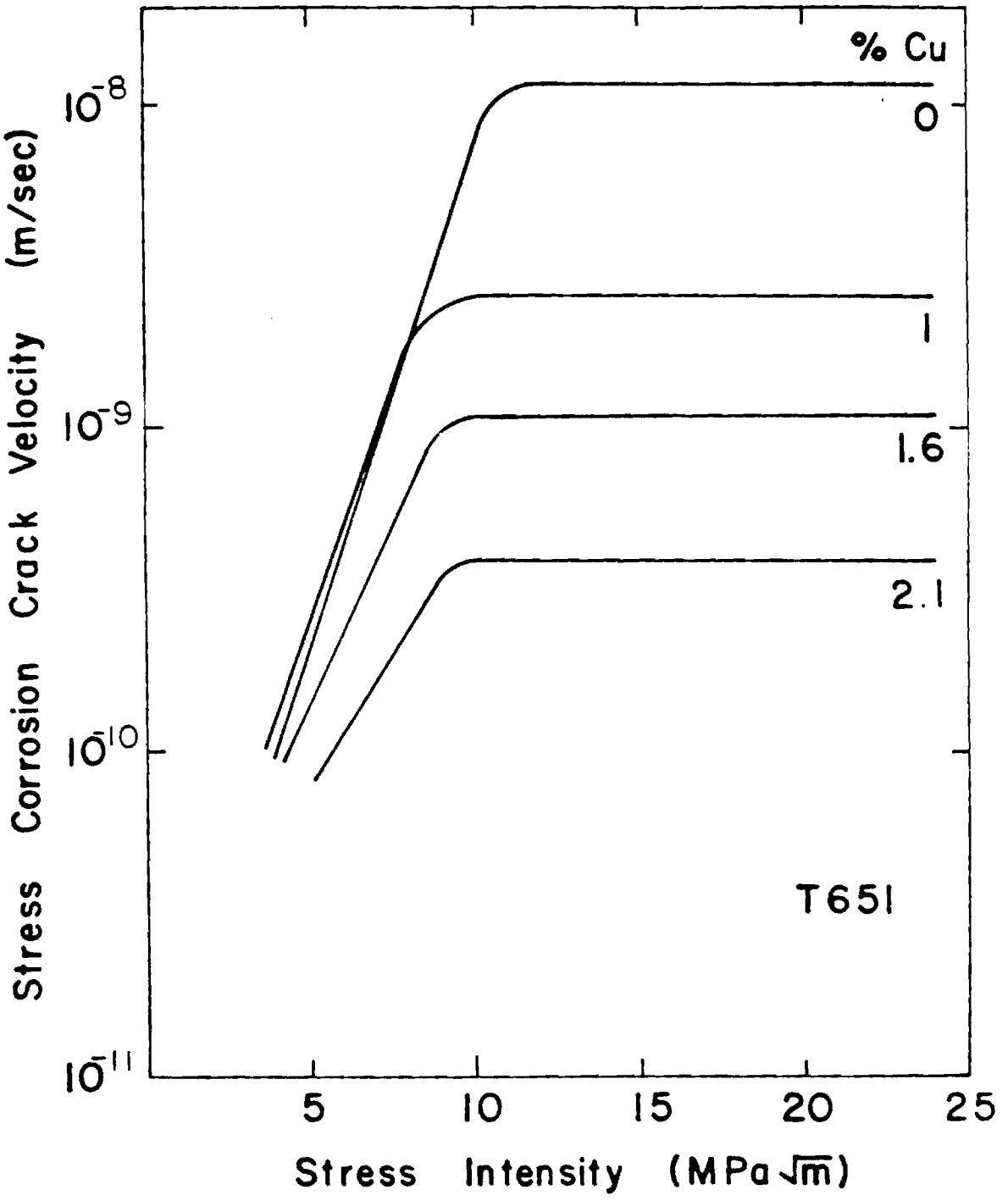

Figure 9. Stress Corrosion Crack Velocity of the Four Experimental Alloys in -T651 Condition as a Function of Stress Intensity.

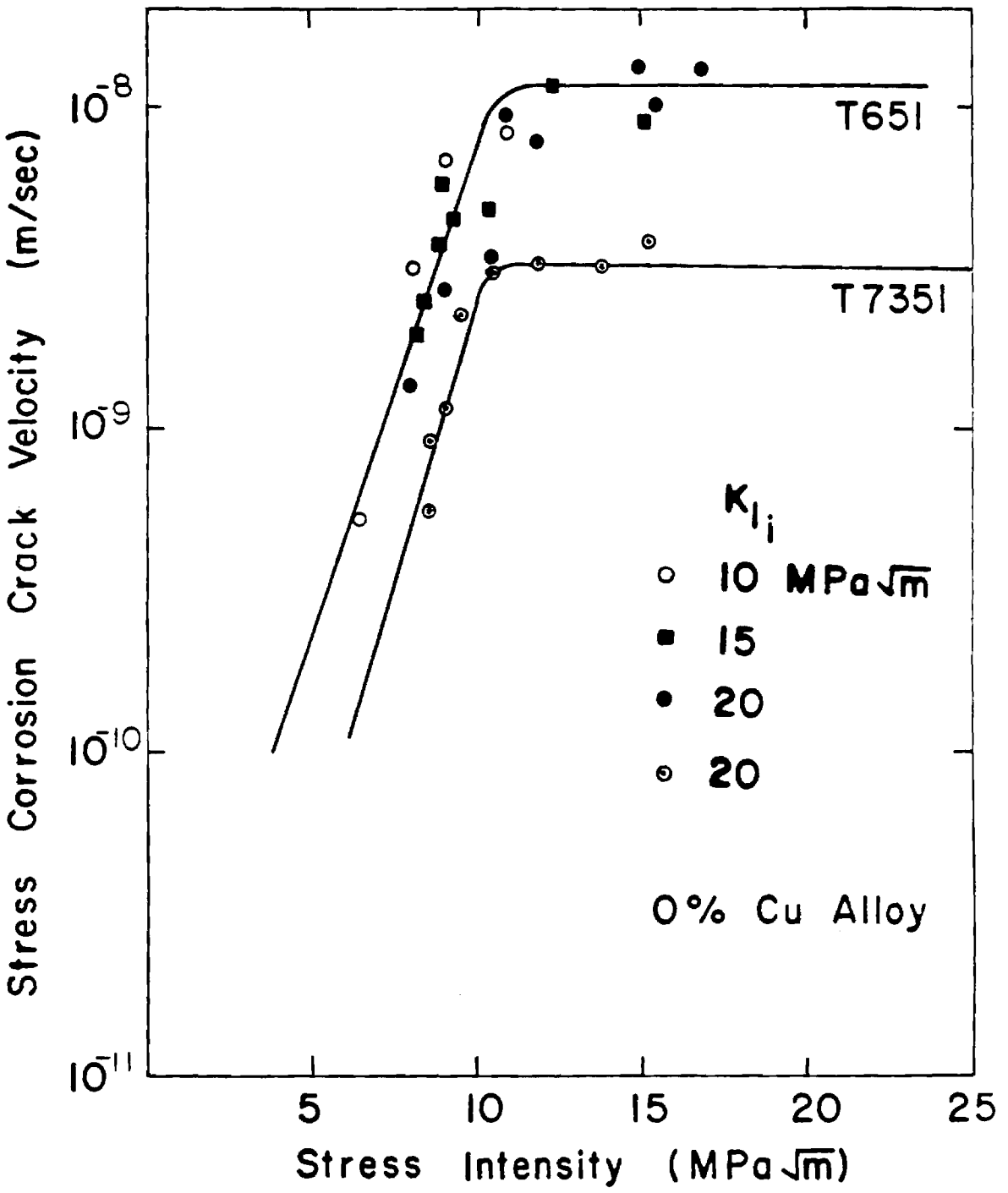

Figure 10. Effect of Overaging on the Stress Corrosion Crack Velocity of the 0% Cu Alloy

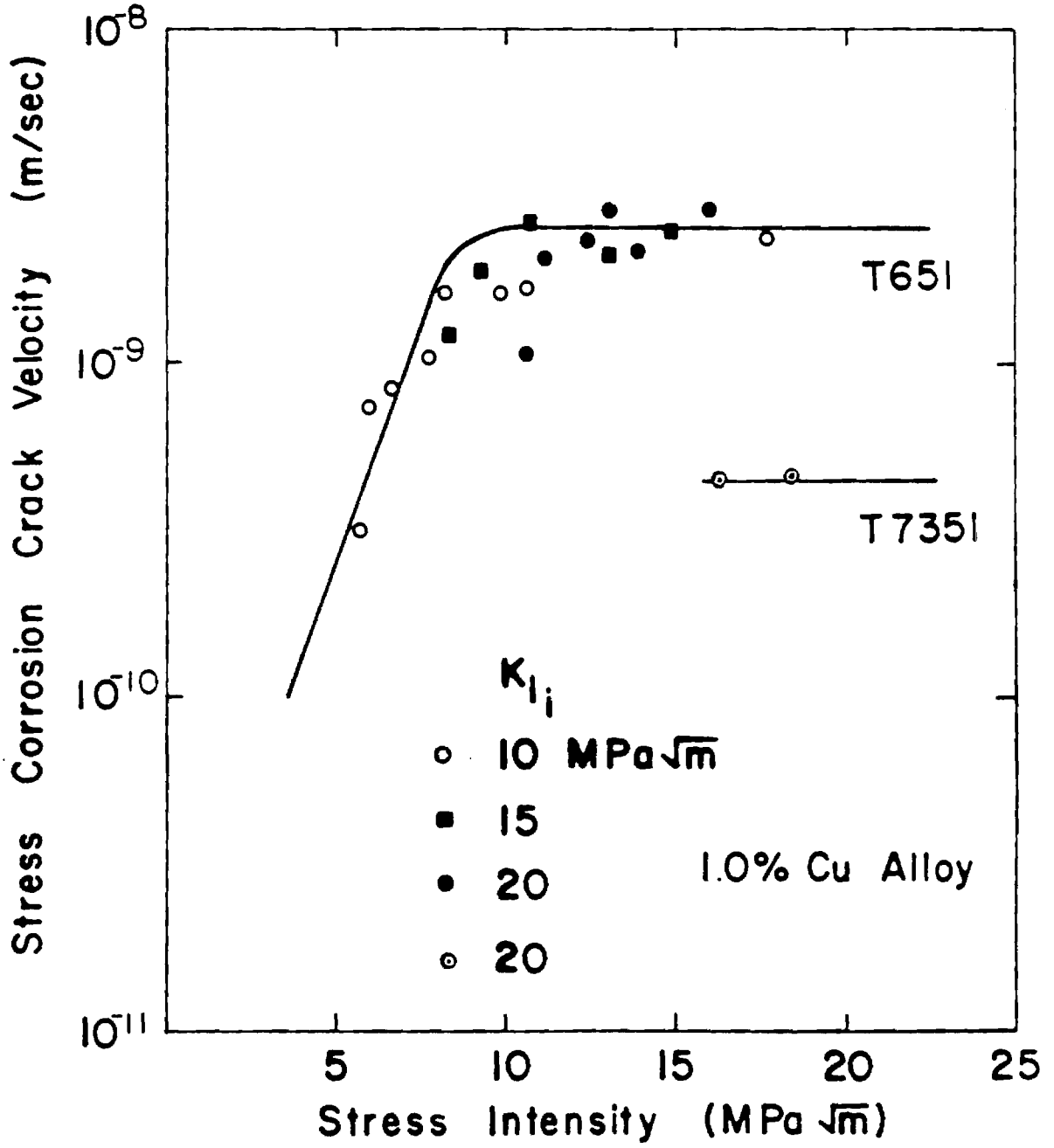

Figure 11. Effect of Overaging on the Stress Corrosion Crack Velocity of 1% Cu Alloy.

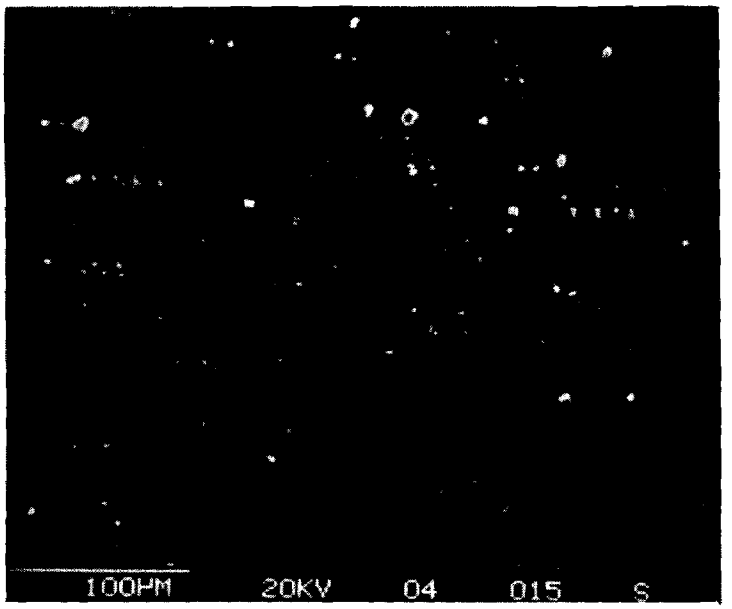

(a)

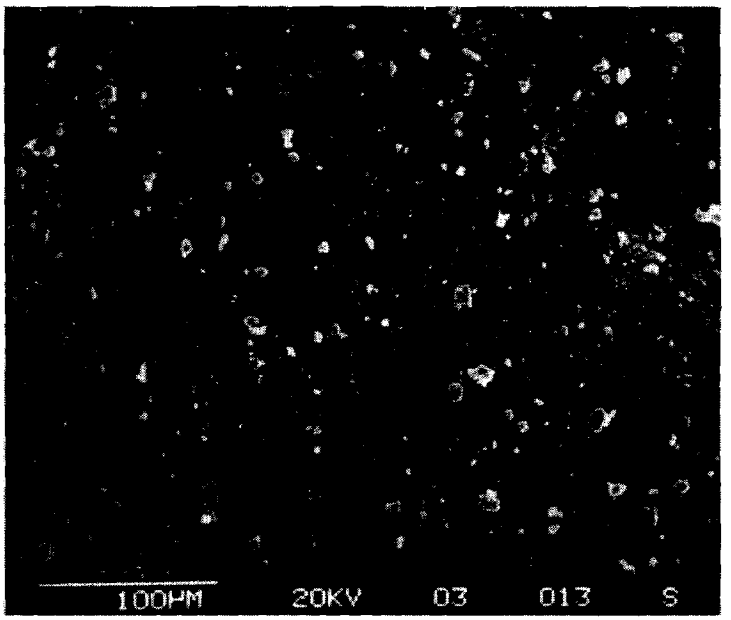

(b)

Figure 12. SEM of Al-Li-Mn alloys showing the size and distribution of Mn precipitates in (a) low Mn alloy and (b) high Mn alloy.

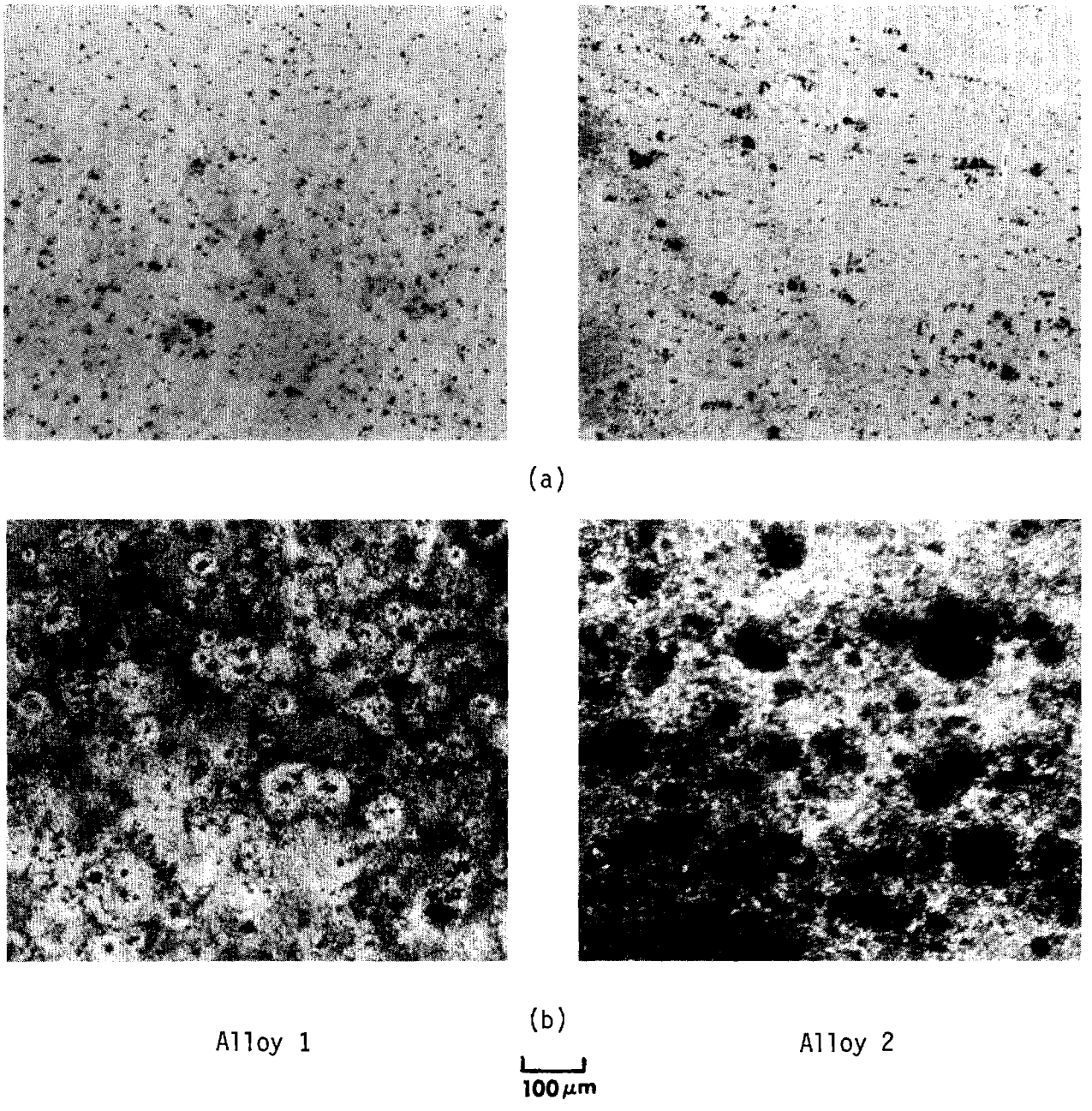

Figure 13. Surface sections of (a) under and (b) overaged specimens after 48 hours in a 3.5% NaCl solution.

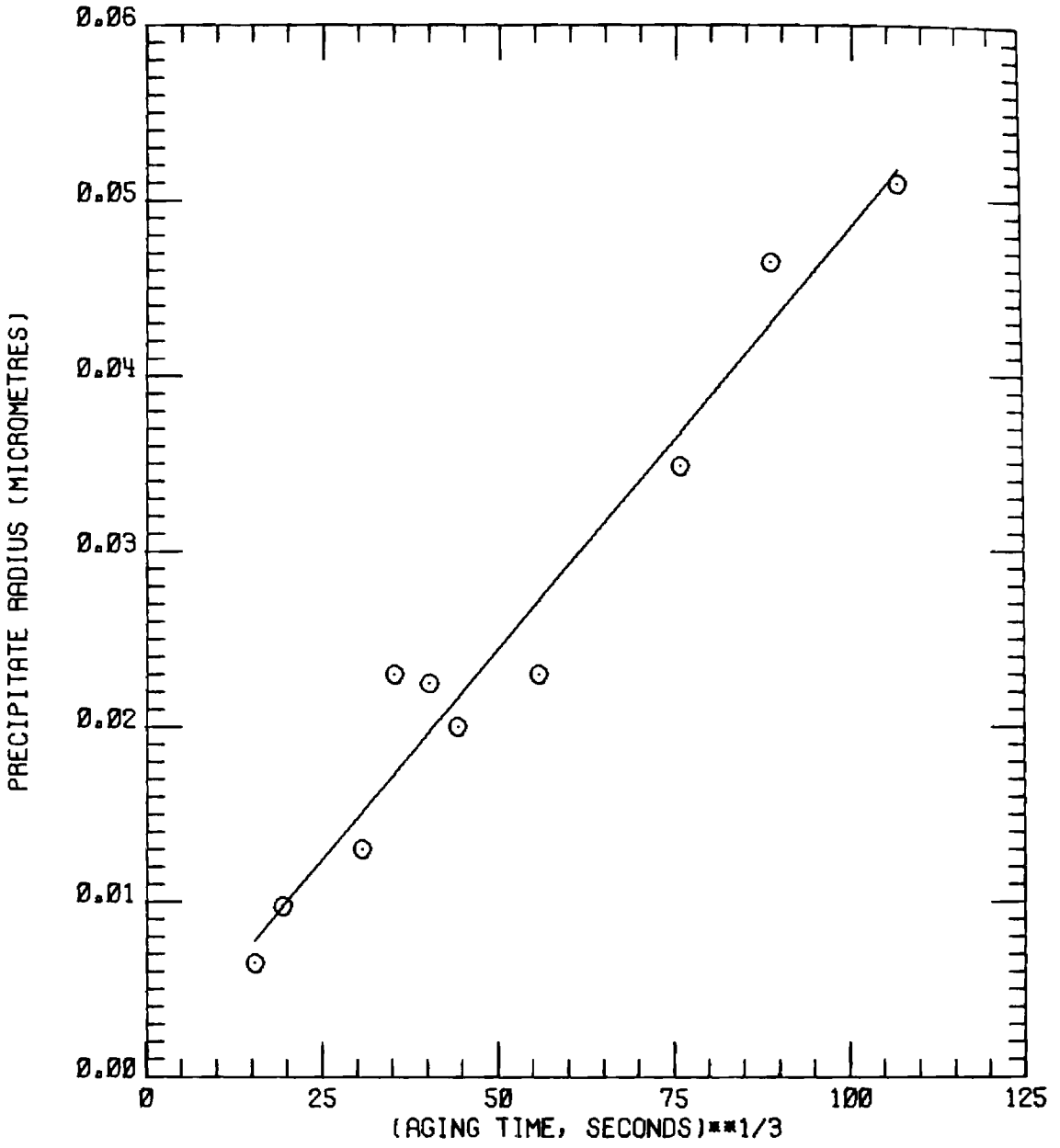

Figure 14. Precipitate radius as a function of isothermal aging time. (Anodized, Polarized light)

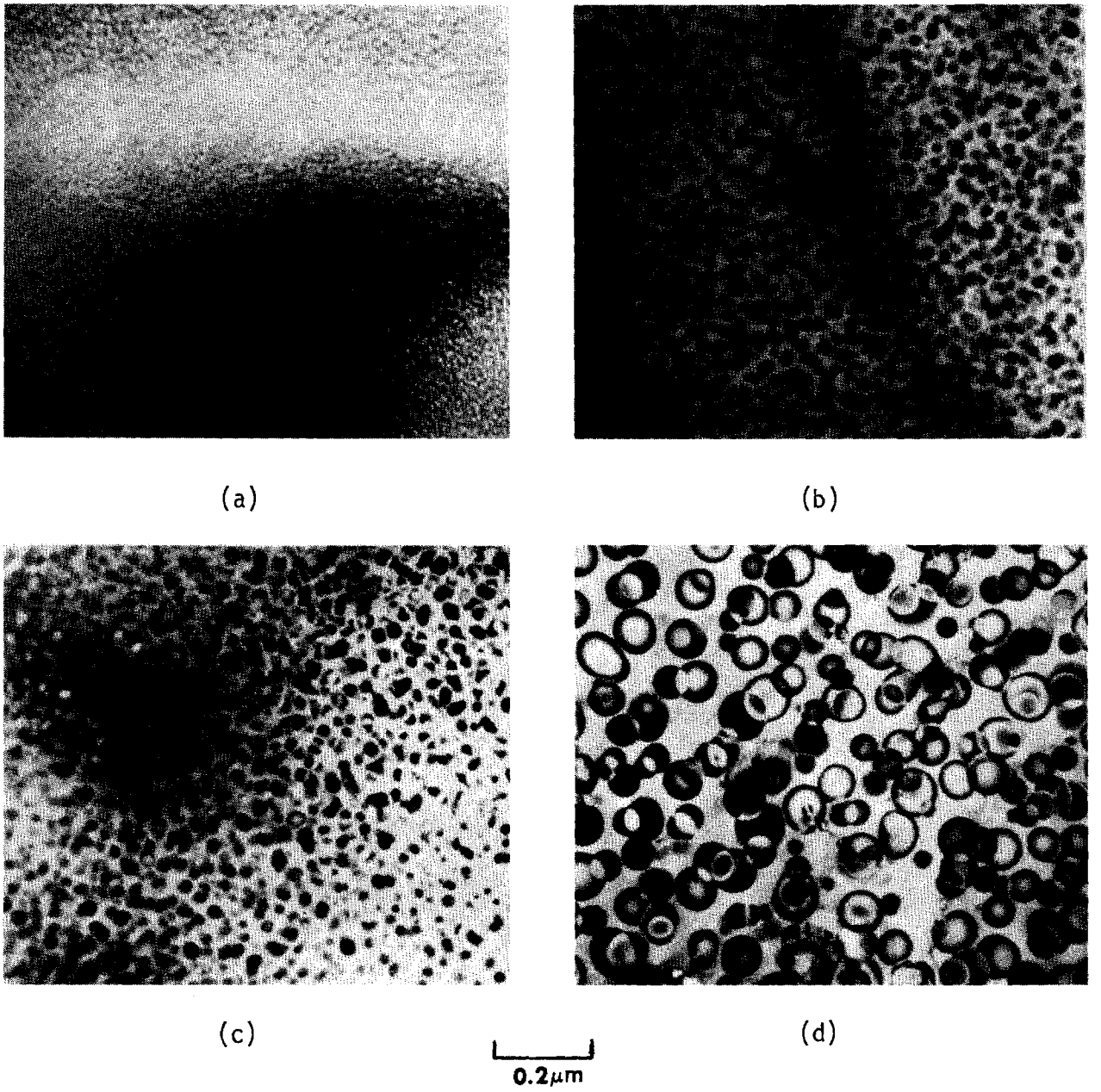

Figure 15. Illustrating the growth of δ' as a function of aging time at 200°C, (a) 0.25 (b) 12 (c) 24 and (d) 336 hours.

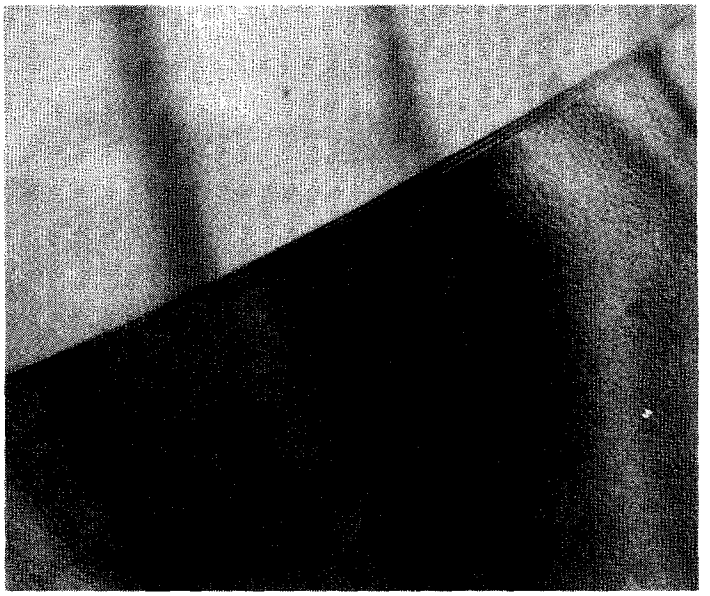

(a)

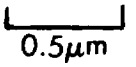

(b)

Figure 16. Representative TEMS showing the development of precipitate free zones of low Mn alloy (a) aged at 0.25 hours, and (b) 336 hours.

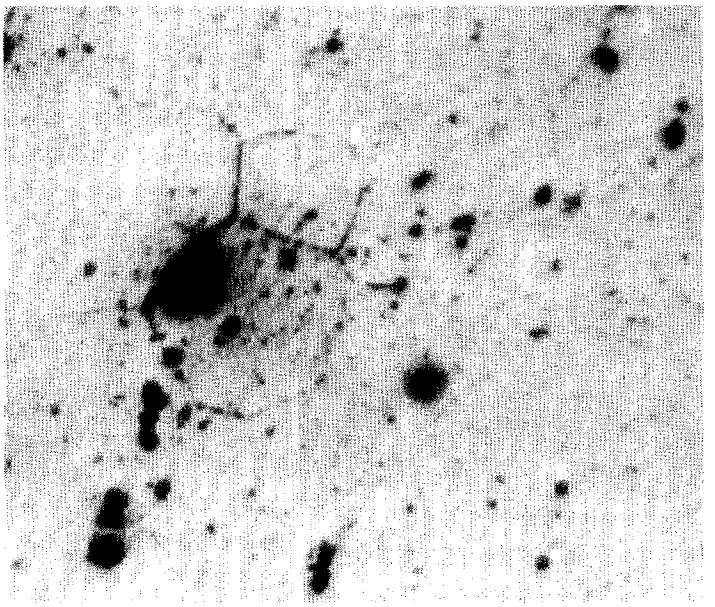

(a)

20μm

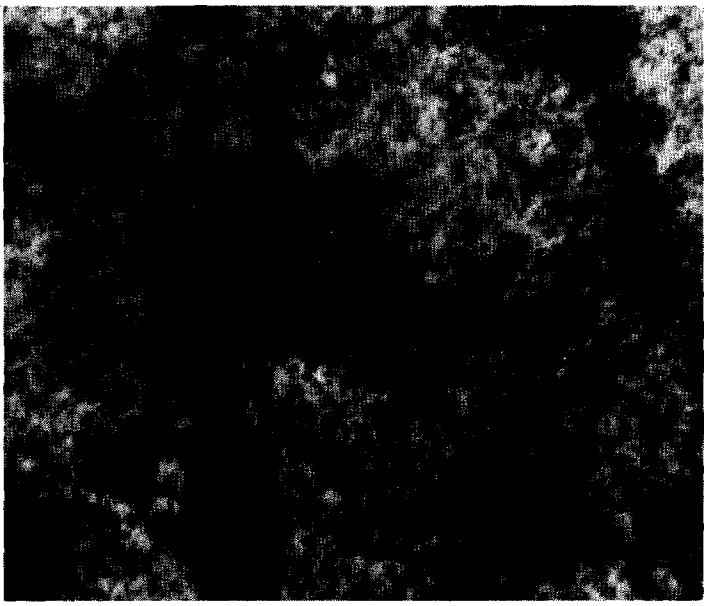

(b)

Figure 17. Optical photomicrographs of the surface of the potentiodynamic anodic polarization specimens, in the (a) under and (b) overaged condition, 1 minute after reaching the breakdown potential. (low Mn alloy)

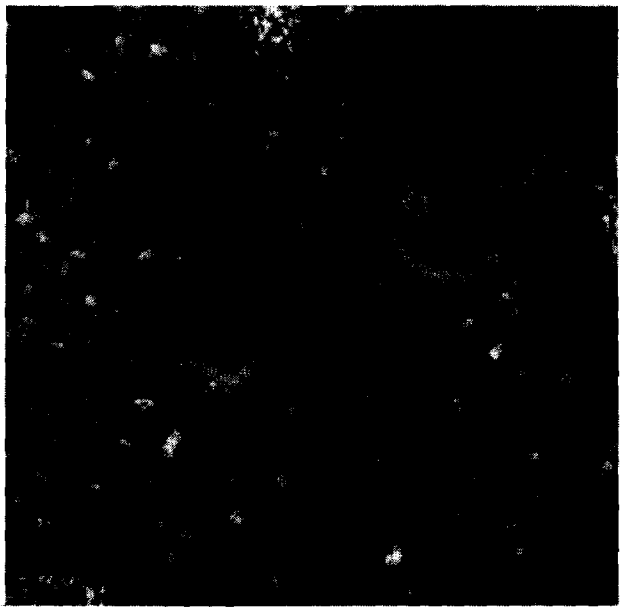

Figure 18. SEM showing the attack after 48 hours in 3.5% NaCl solution at the interface of the secondary intermetallics. (alloy 2, aged 24 hours)

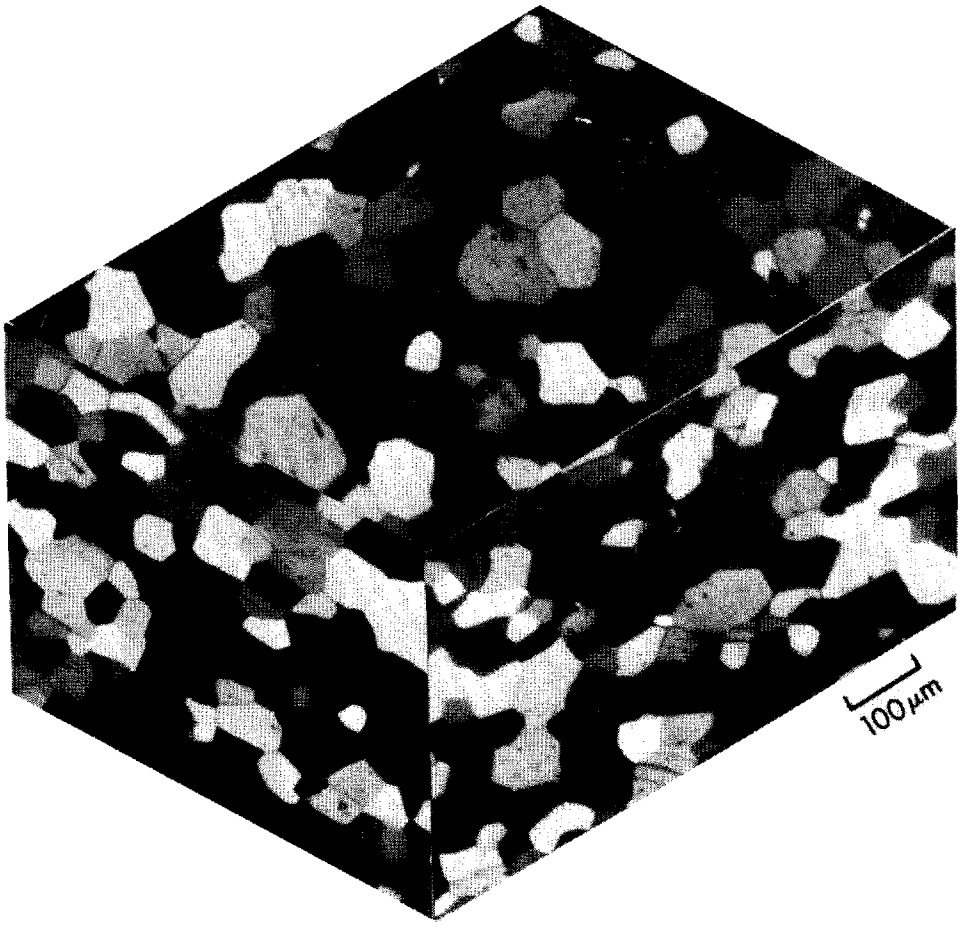

Figure 19. 3 D photomicrograph showing the grain morphology of Alloy 1. (Anodized, polarized light)

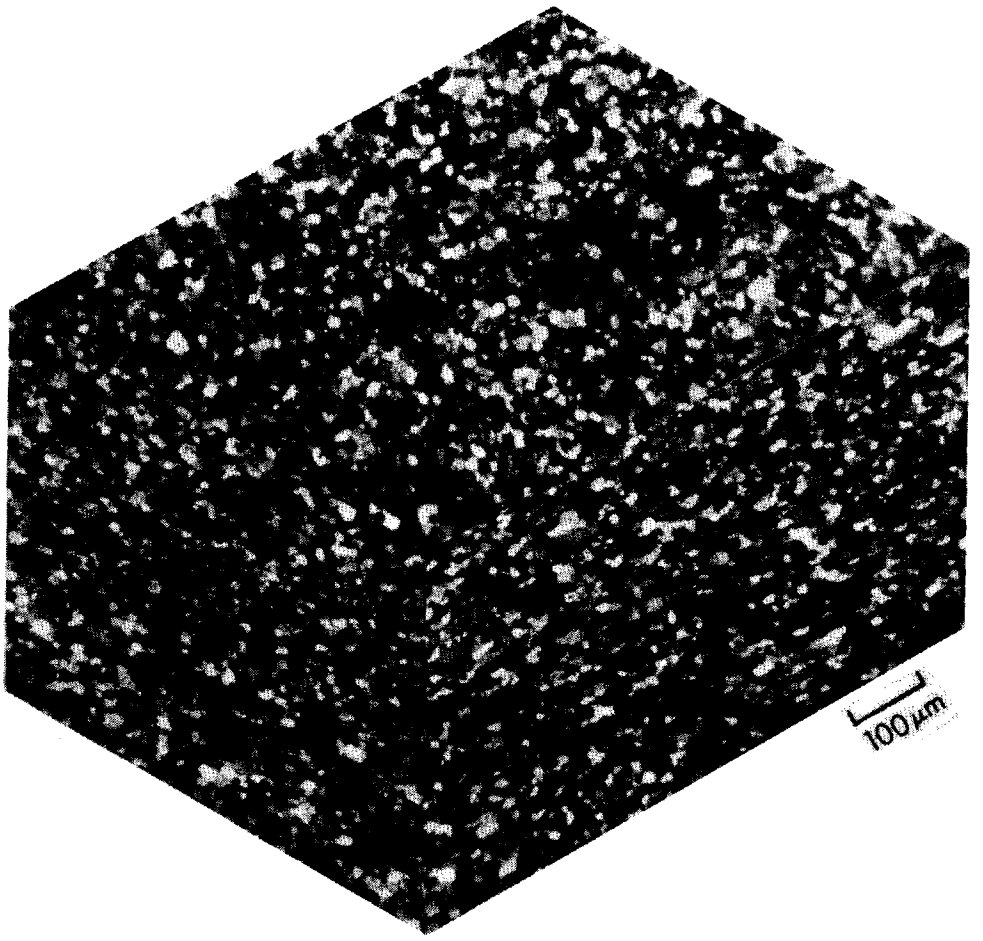

Figure 20. 3 D photomicrograph showing the grain morphology of Alloy 2. (Anodized, polarized light)